Random-diluted triangular plaquette model: Study of phase transitions in a kinetically constrained model

Silvio Franz,[1] Giacomo Gradenigo,[1,2,3,4,*] and Stefano Spigler[1]
[1]*LPTMS, CNRS, Université Paris Sud et Université Paris-Saclay, 91405 Orsay, France*
[2]*IPhT, CEA Saclay, F-91191 Gif-sur-Yvette Cedex, France*
[3]*Université Grenoble Alpes, LIPHY, F-38000 Grenoble, France*
[4]*CNRS, LIPHY, F-38000 Grenoble, France*
(Received 23 July 2015; revised manuscript received 28 January 2016; published 3 March 2016)

We study how the thermodynamic properties of the triangular plaquette model (TPM) are influenced by the addition of extra interactions. The thermodynamics of the original TPM is trivial, while its dynamics is glassy, as usual in kinetically constrained models. As soon as we generalize the model to include additional interactions, a thermodynamic phase transition appears in the system. The additional interactions we consider are either short ranged, forming a regular lattice in the plane, or long ranged of the small-world kind. In the case of long-range interactions we call the new model the random-diluted TPM. We provide arguments that the model so modified should undergo a thermodynamic phase transition, and that in the long-range case this is a glass transition of the "random first-order" kind. Finally, we give support to our conjectures studying the finite-temperature phase diagram of the random-diluted TPM in the Bethe approximation. This corresponds to the exact calculation on the random regular graph, where free energy and configurational entropy can be computed by means of the cavity equations.

DOI: 10.1103/PhysRevE.93.032601

I. INTRODUCTION

There are two main points of view to understand the nature of the glass phase. On one hand there is the idea of "dynamic facilitation," which emphasizes the role of frustration in the dynamics: the motion of the microscopic constituents of a glass-forming system becomes inhibited by their close neighbors when the system is cooled. The consequence is that the material remains stuck for an extremely long time in a certain amorphous configuration. On the other hand there is the landscape scenario, or "random first-order transition" (RFOT) theory [1–4], according to which the formation of a glass is the reflex of the existence of metastable states whose multiplicity is strongly reduced as the temperature is lowered. In the dynamic facilitation scenario thermodynamics is deemphasized and the interaction only plays a role in dynamics. This idea is at the basis of the description of glasses provided by kinetically constrained models (KCMs) [5–10]. KCMs are lattice models where the variables do not have energetic interactions, but are subject to dynamic constraints. Both theories have reference models that reproduce important aspects of glass phenomenology, and it is hard to decide which scenario is the appropriate one to describe real systems. The two descriptions are very similar at the mean-field level: recent numerical simulations have shown that both at the level of average behavior [11] and at the level of fluctuations [12] KCM models on random graphs [13] follow a glass transition pattern predicted by mode-coupling theory. In [14] it was also shown that a typical RFOT model, the XOR-SAT on a random graph, can be mapped in a KCM. The XOR-SAT model combines salient features of both theories: it has a trivial high-temperature thermodynamics as in KCM, but with a finite-temperature entropy crisis glass transition as in RFOT. It is an interesting question whether this commonality of mechanisms observed in the mean field extends to finite dimensions.

To investigate this question, in the present work we analyze the thermodynamic properties of a modified 2D triangular plaquette model (TPM) [15–18]. The original TPM is an example of a KCM: it is a spin model whose thermodynamics is one of a trivial paramagnet while at the same time the model displays dynamical glassy phenomena with a super-Arrhenius relaxation time. Indeed, the TPM is nothing but a realization of the XOR-SAT model in finite (two) dimensions [14]. Our attention was brought to the TPM in particular by the results of [19]. In [19], and more recently in [20], it has been shown that the TPM, in the presence of external fields, supports both dynamic and thermodynamic phase transitions to glassy arrested phases. Emphasis is put in [19,20] on the fact that as soon as such external fields are switched off ergodicity is restored, so that the TPM is just marginally glassy. Looking at the results of [19,20] from another perspective, they provide evidence that the trivial thermodynamics of the TPM can be dramatically altered by means of very small perturbations. Following this line, our purpose here is it to show that the triviality of the TPM thermodynamics is marginal and its physics is close to one of the landscape scenario. We will show that as soon as some new interactions are introduced in the TPM, its thermodynamics cannot be trivial anymore and a phase transition appears in the system. Our results support the point of view that the dynamic facilitation and the landscape scenario should be regarded as complementary rather than alternative.

Specifically, the TPM is a lattice spin model where the spins sit on a two-dimensional triangular lattice endowed with "plaquette" interactions: each plaquette corresponds to the product of the three spins placed at the corners of an upward triangular cell of the lattice. The energy of the model is $\mathcal{H} = -\sum_{\langle ijk \rangle} \sigma_i \sigma_j \sigma_k$, where each triplet $\langle ijk \rangle$ of indices is

*ggradenigo@gmail.com

 ©2016 American Physical Society

associated with a plaquette. The remarkable observation made in [15] is that there is a one-to-one correspondence between spins and plaquettes: a configuration of the system is well defined either assigning the values of the spins $\{\sigma_i\}_{i=1,\dots,N}$ or the values of the plaquette variables $\{\tau_a\}_{a=1,\dots,N}$, where $\tau_a = \sigma_{i(a)}\sigma_{j(a)}\sigma_{k(a)}$. In terms of the plaquette variables the Hamiltonian is equivalent to that of a system of noninteracting spins in a field, for which the partition function can be trivially calculated: $\mathcal{Z} = 2^N[\cosh(\beta)]^N$. The absence of thermodynamic singularities, together with a critical slowing down at low temperatures [15,16], $\tau_{\rm rel} \sim \exp(A/T^2)$, are typical features of KCMs. If one performs local Monte Carlo updates acting upon the spins but then looks at the resulting dynamics of the plaquette variables, the latter looks like a kinetically constrained dynamics. It happens that the annihilation of a "defect," namely the flip of a plaquette a from $\tau_a = -1$ to $\tau_a = 1$, is favored only when there is at least one other defect, i.e., an excited plaquette, connected to a. Two plaquettes are connected when they have a spin in common. Since the dynamics acts upon spins, and in the TPM the update of one spin always corresponds to the update of three plaquettes, the Monte Carlo dynamics corresponds to the flipping of three plaquettes per time. Due to the odd number of plaquettes attached to a spin σ_i, in the TPM there is no spin flip with $\Delta E = 0$, since $E = -\sum_{a\in\partial i}\tau_a$. For the same reason one needs that at least two of the plaquettes attached to σ_i are excited, namely they are both $\tau_a = -1$, in order to have $\Delta E < 0$ by flipping σ_i. This explains why the annihilation of a defect is favored only in the vicinity of another defect. The transition rates for spin updates depend on temperature through the standard Metropolis rule, namely each attempted update is accepted with probability $p = \min(1, e^{-\beta\Delta E})$. The idea we want to test in this paper is that if we introduce some new interactions between variables (or if we remove some), an important parameter in the thermodynamics is the ratio $\alpha = M/N$ between the number M of plaquettes in the Hamiltonian and the number N of spins in the systems. While such a scenario is well established for plaquette models on random graphs [21], this has not been tested to our knowledge in finite-dimensional geometries. Of course the ratio α can be changed in many different ways. Here we will focus on two classes of models with extra plaquettes: in the first class we choose the triplets of spin in the new interactions completely at random; in the second class the new interactions are taken on a regular sublattice of the triangular lattice, either a fraction of them chosen randomly or all the interactions of the sublattice. With the first choice we induce arbitrarily long-range interactions, so that the resulting model is a kind of small-world network [22]. In order to be general, in the model with long-range interactions we also take into account a dilution of the plaquettes of the original two-dimensional triangular lattice: that is why we call such a model the "random-diluted triangular plaquette" model.

The paper is structured as follows. In the first part, Sec. II, we present the two classes of modified TPMs just mentioned. For each class we discuss the behavior of the high-temperature expansion and present the results of numerical simulations. In Sec. III we discuss how to use the leaf-removal algorithm [21], which is a method borrowed from the study of constrained optimization problems, to draw a tentative phase diagram at $T = 0$ of the random-diluted TPM in the (α_s, α_L) plane: α_L is the concentration of long-range plaquettes while α_s is the concentration of short-range plaquettes in the two-dimensional lattice. Finally, in Sec. IV of the paper we present the phase diagram at finite temperature for the random-diluted TPM on the random regular graph, which we will refer to often in the paper also as the Bethe lattice geometry, where the glass transition temperature can be exactly calculated by solving the cavity equations.

II. TRIANGULAR PLAQUETTE MODEL WITH ADDITIONAL INTERACTIONS: HIGH-TEMPERATURE EXPANSION AND NUMERICAL SIMULATIONS

The simplest choice of additional interactions for a modified TPM with Hamiltonian $H = H_{\rm TPM} + H_{\rm extra}$ is represented by new ferromagnetic plaquettes: $H_{\rm extra} = -\sum_{ijk}\sigma_i\sigma_j\sigma_k$. In the Hamiltonian $H_{\rm extra}$ the only source of randomness is then represented by the choice of which spins participate in each of the new plaquettes, i.e., the choice of the triplets of indices ijk. The ground state of the so modified TPMs is the configuration where all spins attain the value $\sigma_i = +1$. The aim of this work is to provide evidence that in some of these modified TPMs a glass transition takes place before the system has the time to relax to the ordered ground state. We already know from the literature that this is the case for the TPM on a random graph [23]. The idea of introducing new interactions is motivated by the purpose of inducing an entropic crisis in the system, which is the typical mechanism for the formation of a glass phase within the RFOT theory scenario [24]. We have already mentioned that in the TPM the partition function is simply $\mathcal{Z} = 2^N[\cosh(\beta)]^N$. Let us assume the existence of a modified TPM such that the number of plaquettes M is different from the number of spins N, but the partition function is still the trivial one: $\mathcal{Z} = 2^N[\cosh(\beta)]^M$. In this hypothetical TPM the entropy of the system would be

$$s(\beta) = \ln(2) + \frac{M}{N}\ln[\cosh(\beta)] - \frac{M}{N}\beta\tanh(\beta), \qquad (1)$$

which in the limit of zero temperature yields

$$\lim_{\beta\to\infty} s(\beta) = \left(1 - \frac{M}{N}\right)\ln(2). \qquad (2)$$

Equation (2) tells us that in the case when $\alpha = M/N > 1$ the entropy is negative at $T = 0$, so that an entropic crisis takes place at $T > 0$. Clearly, since the TPM and any decoration of it are models with discrete variables, any expression yielding a negative entropy cannot be an exact one. The only possibility is that, in a TPM with additional plaquettes $(M/N > 1)$, the expression of the entropy in Eq. (1) is an approximated one; for instance it can be the one provided by high-temperature expansion. This expansion usually well describes the properties of the liquid phase: the finding of a negative entropy by its prolongation to low temperatures tells us that the description of the system as in the liquid state becomes inconsistent and the glass comes into play [24]. Our purpose here is to show that, in some modified TPMs, the parameter which controls the entropy crisis in the high-temperature phase is the ratio $\alpha = M/N$ between the number of plaquettes and the number of spins. While it is

well known for mean-field plaquette models that the glass transition is controlled by such a ratio $\alpha = M/N$ [21], we provide here some evidence that this should be the case also in finite dimensions. All the TPMs with additional interactions we discuss here are characterized by a Hamiltonian of the kind

$$H = H_{\rm TPM} + H_{\rm extra}, \tag{3}$$

where two different contributions are read off: $H_{\rm extra} = -\sum_{r=1}^{M_L} \sigma_{i_r}\sigma_{j_r}\sigma_{k_r}$, with the index r running over the new additional plaquettes, and the standard Hamiltonian of the TPM model, $H_{\rm TPM} = -\sum_{s=1}^{M_s} \sigma_{i_s}\sigma_{j_s}\sigma_{k_s}$, with the index s running over the plaquettes of the two-dimensional triangular lattice. The two parameters which characterize the model are the concentrations of original TPM plaquettes and of new additional plaquettes: respectively $\alpha_s = M_s/N$ and $\alpha_L = M_L/N$.

The models with additional plaquettes connecting arbitrarily far apart spins and those with additional short-range plaquettes will be presented respectively in Sec. II A and Sec. II B. In Sec. II A and Sec. II B we study the high-temperature expansion and present some numerical results for the simplest case in which α_L is arbitrary but α_s is fixed to $\alpha_s = 1$, that is, when there is no dilution of the plaquettes in the original 2D triangular lattice. Since the analysis of Sec. II A and Sec. II B shows that the best candidate to display a low-temperature glass transition is the TPM model with additional long-range plaquettes ("small-world" network), this model will be studied in the rest of the paper (Sec. III and Sec. IV), also taking into account values $\alpha_s < 1$. The model in which both α_s and α_L take values in the interval $[0,1]$ is the random-diluted TPM.

A. Long-range additional plaquettes: The random-diluted TPM

A generalized TPM with additional plaquettes has the following high-temperature expansion for the partition function:

$$\mathcal{Z} = 2^N[\cosh(\beta)]^M\left(1 + \sum_{m=1}^{M} \mathcal{C}(m,M)[\tanh(\beta)]^m\right), \tag{4}$$

where the sum on the right-hand side of Eq. (4) runs over *hyperloops* [25] made of m plaquettes: $\mathcal{C}(m,M)$ represents the number of hyperloops of m plaquettes that can be built in a system with a total number M of plaquettes. A hyperloop is defined [25] as a set of interactions such that each spin is appearing an even number of times. The precise expression of $\mathcal{C}(m,M)$ depends on the model. For instance, in the pure TPM, one has $\mathcal{C}(m, M = N) = 0$ and the high-temperature series yields exactly the partition function. Other situations will be discussed in the following paragraphs. Let us focus here on the behavior of the high-temperature expansion in the case when the $M_L = \alpha_L N$ plaquettes of $H_{\rm extra}$ have spins drawn with uniform probability from the lattice, with the only constraint that spins in the same plaquette are different. Let us indicate with $\mathcal{R}$ an instance of disorder, namely a particular choice of the triplets of spins in the plaquettes of $H_{\rm extra}$. It is also convenient to introduce the average of a function $f[\boldsymbol{\sigma}]$, with $\boldsymbol{\sigma}$ denoting a configuration of the system $\boldsymbol{\sigma} = (\sigma_1, \ldots, \sigma_N)$, with respect to the measure provided by the pure TPM:

$$\langle f[\boldsymbol{\sigma}]\rangle_{\rm TPM} = \frac{1}{\mathcal{Z}_{\rm TPM}} \sum_{\boldsymbol{\sigma}} e^{-\beta H_{\rm TPM}[\boldsymbol{\sigma}]} f[\boldsymbol{\sigma}]. \tag{5}$$

The partition sum for a given $\mathcal{R}$ reads then

$$\begin{aligned}
\mathcal{Z}_{\mathcal{R}} &= \sum_{\sigma} e^{-\beta H_{\rm TPM}[\boldsymbol{\sigma}] + \beta \sum_r^{M_L} \sigma_{i_r}\sigma_{j_r}\sigma_{k_r}} \\
&= 2^N[\cosh(\beta)]^{N+M_L}\left\langle \prod_r [1 + \sigma_{i_r}\sigma_{j_r}\sigma_{k_r}\tanh(\beta)]\right\rangle_{\rm TPM} \\
&= 2^N[\cosh(\beta)]^{N+M_L}\Bigg[1 + \sum_{r\in\mathcal{R}}^{M_L}\langle\tau_r\rangle_{\rm TPM}\tanh(\beta) \\
&\quad + \sum_{r\neq p\in\mathcal{R}}^{M_L}\langle\tau_r\tau_p\rangle_{\rm TPM}[\tanh(\beta)]^2 + \cdots\Bigg],
\end{aligned} \tag{6}$$

where, to lighten the notation, we used the plaquette variables $\tau_r = \sigma_{i_r}\sigma_{j_r}\sigma_{k_r}$ and M_L is the number of additional plaquettes in $H_{\rm extra}$. From Eq. (6) we see that the product of m "long-range" plaquettes contributes a hyperloop in the high-temperature expansion if and only if in the original TPM the corresponding correlation function $\langle\sigma_{i_1}\sigma_{j_1}\sigma_{k_1}\ldots\sigma_{i_m}\sigma_{j_m}\sigma_{k_m}\rangle_{\rm TPM}$ is finite in the thermodynamic limit.

Let us now notice that in our modified TPM with long-range plaquettes the annealed and quenched averages are equivalent at high temperature due to the fact that the partition function is self-averaging, i.e., $\overline{\mathcal{Z}}^2 = \overline{\mathcal{Z}^2}$: the proof of self-averaging is presented in Appendix A. This equivalence of annealed and quenched averages in the high-temperature phase is typical not only of the random energy model [26], the simplest model with an entropy-driven glass transition like the one we expect in our modified TPM, but also of all the p-spin models fully connected or on a random (hyper)graph. In all these situations the behavior of the thermodynamic potentials in the high-temperature phase is obtained from the annealed free energy $f = -(\beta N)\ln(\overline{\mathcal{Z}})$. We are therefore allowed to average over disorder the partition function:

$$\begin{aligned}
\overline{\mathcal{Z}} &= \frac{1}{\mathcal{N}(\mathcal{R}_M)}\sum_{\mathcal{R}_M}\mathcal{Z}_{\mathcal{R}} \\
&= 2^N[\cosh(\beta)]^{N+M_L}\Bigg[1 + \frac{\binom{M_L}{1}}{\mathcal{N}(\mathcal{R}_1)}\sum_{r=1}^{\mathcal{N}(\mathcal{R}_1)}\langle\tau_r\rangle_{\rm TPM}\tanh(\beta) \\
&\quad + \frac{\binom{M_L}{2}}{\mathcal{N}(\mathcal{R}_2)}\sum_{r,p=1}^{\mathcal{N}(\mathcal{R}_1)}\langle\tau_r\tau_p\rangle_{\rm TPM}[\tanh(\beta)]^2 + \cdots\Bigg].
\end{aligned} \tag{7}$$

In Eq. (7) the indices r, p run over the set of all possible choices of random triplets of spins, while $\mathcal{N}(\mathcal{R}_k)$ is the number of ways in which k random triplets can be chosen, which, in the limit $N \gg k \gg 1$, reads

$$\mathcal{N}(\mathcal{R}_k) = \binom{N}{3}^k \sim O(N^{3k}). \tag{8}$$

In each sum on the right-hand side of Eq. (7) the number of choices for the plaquettes not appearing in the brackets $\langle\,\rangle_{\rm TPM}$ has been canceled out with the corresponding factor in

the normalization constant. The binomial coefficient in front of each summation symbol in Eq. (7) represents the number of ways to choose m plaquettes out of M_L. Taking then into account that the typical value $\langle \tau_r \tau_p \tau_q \rangle_{\text{TPM}}$ does not depend on the choice of the indices, the expression in Eq. (7) simplifies to

$$\mathcal{Z} = 2^N [\cosh(\beta)]^{N+M_L} \times \left[1 + \sum_{m=1}^{M_L} \binom{M_L}{m} \langle \tau_1 \dots \tau_m \rangle_{\text{TPM}} [\tanh(\beta)]^m \right]. \quad (9)$$

It can be then proven, as shown in Appendix A, that

$$\lim_{N\to\infty} \binom{M_L}{m} \langle \tau_1 \dots \tau_m \rangle_{\text{TPM}} = 0, \quad (10)$$

so that the high-temperature expansion is trivial and we have

$$\overline{\mathcal{Z}} = 2^N [\cosh(\beta)]^{N+M_L}. \quad (11)$$

The consequence of Eq. (11) is that, since $\alpha = (N + M_L)/N > 1$, according to the expression in Eq. (2), at $T = 0$ the entropy is negative, which in turn implies an entropic crisis at $T > 0$. As already mentioned, the finding of negative entropy is, for a model like ours with discrete variables, an artifact of the high-temperature expansion: a phase transition usually takes place preventing this from happening. Such a phase transition is not necessarily a glass one: indeed we find from the numerical simulations discussed below that a first-order transition to an ordered state is taking place. As shown in [23] for a TPM on a random graph, the presence of an ordered ground state does not spoil the possibility of a glass transition.

Numerical simulations. In order to test the behavior of the TPM in the presence of extra plaquettes with randomly chosen spins we realized numerical simulations of the model. We studied a lattice with triangular cells and the shape of a rhombus with $L = 128$ plaquettes per side, periodic boundary conditions, and a concentration of extra random plaquettes $\alpha_L = 0.1$. In order to speed up the equilibration dynamics at low temperatures we used a rejection-free algorithm [27]. The behavior of the internal energy along a hysteresis cycle is represented by the data in Fig. 1. The scenario is as follows. By cooling down the system from high temperatures one first finds a spinodal temperature T_s where an ordered metastable state appears. By further cooling the systems a melting temperature T_m where the ordered state becomes stable is found. The melting temperature has been determined from the free energy obtained numerically via thermodynamic integration: $f(\beta_1) = \beta_0 \beta_1^{-1} f(\beta_0) + \beta_1^{-1} \int_{\beta_0}^{\beta_1} d\beta e(\beta)$. In panel (a) of Fig. 1 there are two data sets which correspond respectively to the paramagnetic phase, at the higher energy $e^{\text{para}}(\beta)$, and the ordered phase, at the lower energy $e^{\text{ferro}}(\beta)$; these two phases are stable respectively above and below the melting temperature T_m. By independently performing the thermodynamic integration over $e^{\text{para}}(\beta)$ and $e^{\text{ferro}}(\beta)$ one gets respectively $f^{\text{para}}(\beta)$ and $f^{\text{ferro}}(\beta)$; T_m is determined by the crossing of $f^{\text{para}}(\beta)$ and $f^{\text{ferro}}(\beta)$. Since for $T > 1$ data are well interpolated by the high-temperature expansion, we fix the integration constant $f(\beta_0)$ to $f(\beta_0) = -\beta_0 \ln(2) - \beta_0(1 + \alpha_L) \ln[\cosh(\beta_0)]$, with $\beta_0^{-1} = 1.2$. In the top panel of Fig. 1, the melting temperature T_m is represented by a vertical dotted line; it is interesting to note that the system can be cooled to a remarkable extent below T_m while remaining in the disordered liquid phase. Bringing T down further, the relaxation time becomes so large that the system falls out of equilibrium. Our cooling protocol is represented by runs ranging from 10^6 to 10^7 Monte Carlo sweeps for each temperature, and by temperature jumps of $\Delta T = 0.04$. Using this protocol we were not able to detect any tendency of the system to relax to the ordered ground state. From simulations we learn therefore that a first-order transition is present at T_m, but the systems is highly stable in the supercooled liquid phase, namely at temperatures $T < T_m$. This finding suggests that the system avoids on the time scales we sampled the negative entropy obtained by extrapolating the high-temperature expansion just by forming a glass. Let us also note that the annealed high-temperature expansion in Eq. (11) has a very good agreement with simulations; in Fig. 1 it can be seen that within the whole range of temperatures where we could equilibrate the system no relevant departure of data from the annealed energy $e(\beta) = -(1 + \alpha_L) \tanh(\beta)$ can be detected. In Fig. 1 we can also see that the temperature T_0 of the entropy crisis, as can be estimated from the high-temperature expansion of the entropy in Eq. (1), lies below the temperature range where we can equilibrate the system. With respect to the ideal glass transition temperature T_K, the temperature T_0 can be regarded as a lower bound for the possible values of T_K. It is hard to prove or disprove the existence of an ideal glass transition for our modified TPM solely on the basis of numerical data; this

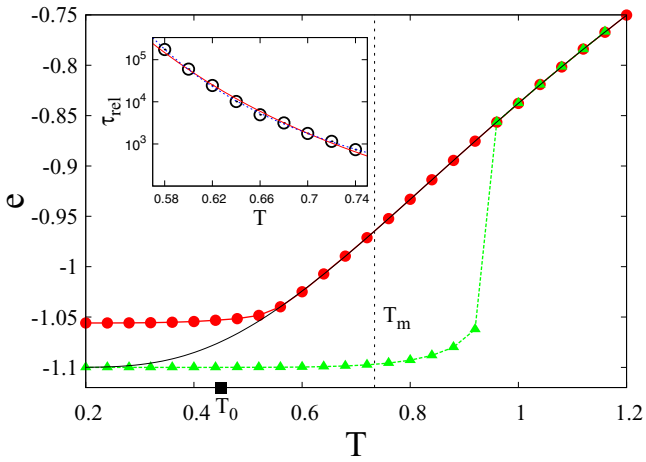

FIG. 1. Main: Energy hysteresis cycle for a TPM model with additional long-range plaquettes. We simulated the model on a lattice with the shape of a rhombus (see for instance the representation of Fig. 2) with $L = 128$ plaquettes per side and a concentration of additional plaquettes $\alpha_L = 0.1$. Red circles: Cooling (cooling rate from 10^6 to 10^7 Monte Carlo steps per $\Delta T = 0.04$). Green triangles: Heating. Continuous black line: High-temperature expansion, $e(T) = -(\alpha_L + 1) \tanh(1/T)$. The melting temperature T_m is indicated by the dotted vertical line while the temperature T_0 of the entropy crisis of the high-temperature expansion is the filled black square. Inset: Circles show relaxation time in the supercooled liquid phase as a function of T, and lines are respectively the two-parameter fit with $a \exp(b/T)$ (continuous red line) and the three-parameter fit with $c \exp[d/(T - T_K)]$. The critical temperature obtained from the fit is $T_K = 0.374$.

is clear looking, for instance, at the inset of the top panel of Fig. 1, where the equilibrium relaxation time $\tau_{\rm rel}$ is shown as a function of temperature. Good fits of the data (see the inset of the top panel in Fig. 1) can be obtained either with a function diverging at finite temperature, $\tau_{\rm rel} \sim \exp[A/(T - T_K)]$, or with the super-Arrhenius law $\tau_{\rm rel} \sim \exp(B/T^2)$ (where clearly $A \neq B$); this is an ambiguous situation that is well known for these kinds of models [28] and in general for glasses. That is why, in order to have better insight into the thermodynamics of the TPM with random plaquettes, we propose in Sec. III a different approach based on tools and ideas borrowed from the study of constraint satisfaction problems.

B. Short-range additional plaquettes

In the previous section we studied the effect of long-range random interactions on the high-temperature expansion of the triangular plaquette model. It is then interesting to investigate what happens in the presence of short-range interactions. Our choice for the new kind of short-range interactions has been guided by the purpose to reduce as much as possible the corrections to the high-temperature expansion. Since in the TPM the correlation of any group of three spins placed at the corners of an equilateral triangle of side 3 is zero [15,16], we defined an additional sublattice formed by equilateral triangular cells of that kind. The additional plaquettes appearing in $H_{\rm extra}$ are then chosen as all the plaquettes of this regular sublattice. In this case we know that at least the first term of the high-temperature expansion vanishes. A representation of this odd sublattice is given in Fig. 2, where the additional plaquettes correspond to the spins placed at the corners of equilateral triangles with side 3. Let us then rewrite the partition function as a series in $\tanh(\beta)$:

$$\mathcal{Z} = 2^N [\cosh(\beta)]^{N+M_L} \Bigg[1 + \sum_{r}^{M_L} \langle \tau_r \rangle_{\rm TPM} \tanh(\beta) + \sum_{r \neq p}^{M_L} \langle \tau_r \tau_p \rangle_{\rm TPM} [\tanh(\beta)]^2 + \cdots \Bigg], \tag{12}$$

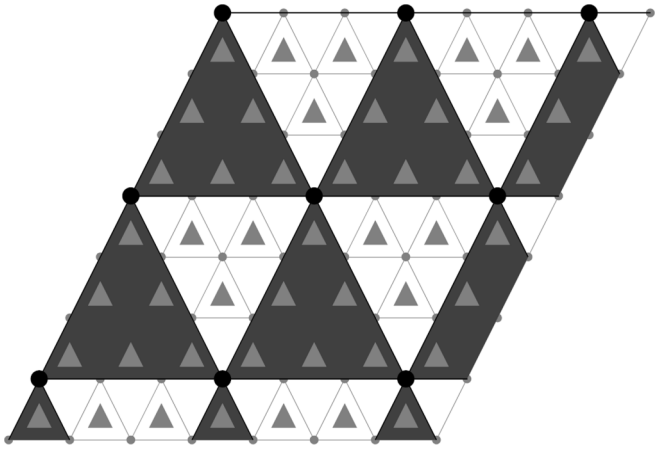

FIG. 2. Triangular lattice for the generalized TPM with additional short-range plaquettes on a regular sublattice made of equilateral triangles of side 3. The original TPM plaquettes and additional interactions are shown as light gray and dark gray triangles, respectively.

where the sums in Eq. (12) run over all the plaquettes of the odd sublattice. At this stage the expression in Eq. (12) is exact; it is just a way of rewriting the partition function. The difference between Eq. (12) above and Eq. (7) in the previous section is that in Eq. (12) each term of the kind

$$\sum_{r_1,\ldots,r_k}^{M_L} \langle \tau_{r_1} \ldots \tau_{r_k} \rangle_{\rm TPM} [\tanh(\beta)]^k \tag{13}$$

accounts for the hyperloops made with all the possible choices of k plaquettes from the additional sublattice, while in Eq. (7) only the hyperloops coming from a given random choice of the additional plaquettes, denoted with $\mathcal{R}$, were taken into account. Due to the regular structure of both the TPM lattice and of the sublattice of additional interactions the existence of finite hyperloops can be proved along the following lines. Let us consider a lattice, TPM plus regular sublattice, of finite size, with open boundary conditions. Think for instance that our system is the portion of the lattice in Fig. 2 which includes the 4 additional plaquettes there represented and the 36 corresponding plaquettes of the TPM, for a total number of $M = 40$ plaquettes. With open boundary conditions, the number of spins in this system is $N = 49$. In this case nothing forbids the partition function to be exactly $\mathcal{Z} = 2^N [\cosh(\beta)]^M$, since at zero temperature the corresponding entropy is positive: $s(T = 0) = 1 - 40/49 > 0$. In this case there is no constraint implying the presence of hyperloops: it might be that for a lattice of this size there is no finite hyperloop. If we think in general to a lattice with the shape of a rhombus, with the same number L of TPM plaquettes on the horizontal and oblique side (consider Fig. 2 to have an idea), and with open boundary conditions, its partition function in absence of hyperloops is

$$\mathcal{Z} = 2^{(L+1)^2} [\cosh(\beta)]^{L^2 + (L/3)^2}. \tag{14}$$

Due to the open boundary conditions, if the number of plaquettes on each row is L the number of spins on the same row is $L + 1$. On the other hand there are $L/3$ rows of additional plaquettes, each with $L/3$ plaquettes. This explains why the total number of spins is $(L + 1)^2$ and why the total number of plaquettes is $L^2 + (L/3)^2$. For simplicity, let us consider just the case when $L = 3m$, where the integer number m indicates therefore the number of plaquettes from the additional sublattice in a row: the zero-temperature entropy per degree of freedom corresponding to the free energy in Eq. (14) is

$$s(T = 0) = 1 - \frac{10m^2}{(3m + 1)^2}. \tag{15}$$

From Eq. (15) we find the maximum value of the parameter m for which is possible to not have hyperloops in the partition function: $m^* = 6$. For $m > m^*$ the expression of $s(T = 0)$ in equation Eq. (15) is negative; this actually proves (the system has discrete variables) that for any lattice of size $m > m^*$ there must be hyperloops in the system. This way of reasoning allows one to prove not only that finite hyperloops are present, but also to fix an upper bound for the size of the smallest hyperloop. Since in a lattice with $m^* + 1 = 7$ there is necessarily a hyperloop, then the smallest hyperloop cannot have more than $(m^* + 1)^2 = 49$ plaquettes taken from the additional sublattice. Let us now explain why in this case there are nontrivial contributions to the high-temperature expansion. In order to

be general, we assume the smallest hyperloops are made of k additional plaquettes of the sublattice and by m plaquettes of the original TPM lattice. For every correlation function of k' plaquettes such that k' is a multiple of k, and the plaquettes are all taken from the sublattice of additional ones, one must take into account disconnected hyperloops. The leading contribution of this kind of term to the high-temperature expansion is

$$\mathcal{Z} = 2^N[\cosh(\beta)]^{N+M_L}\big[1 + M_L[\tanh(\beta)]^{k+m} + M_L(M_L-k)[\tanh(\beta)]^{2k+2m} + M_L(M_L-k)(M_L-2k)[\tanh(\beta)]^{3k+3m}\ldots\big], \quad (16)$$

where $M_L = \alpha_L N$. An explicit expression for the combinatorial prefactor $\mathcal{C}(m,M)$ appearing in Eq. (4) can be provided for the terms appearing in Eq. (16). Let us indicate with $\mathcal{C}(m_{\rm TPM}+m_{\rm extra},M)$ the combinatorial factor which accounts for the multiplicity of a hyperloop with $m_{\rm TPM}$ plaquettes from the original TPM model and $m_{\rm extra}$ additional plaquettes. Then, according to the expression in Eq. (16) and taking n a positive integer we can write

$$\mathcal{C}(kn + m_{\rm TPM}, M) \sim M^n. \quad (17)$$

The series in Eq. (16) can be summed leading to

$$\mathcal{Z} \sim 2^N[\cosh(\beta)]^{N+M_L} e^{\alpha_L N[\tanh(\beta)]^{k+m}}, \quad (18)$$

which represents the contribution to the high-temperature expansion provided by k plaquettes connected hyperloops. We can conclude that in the TPM the addition of short-range additional plaquettes always introduces corrections to the high-temperature series; it is then hard to say whether or not this expansion, which well reproduces the properties of the system in the liquid phase, has positive entropy at all temperatures. What numerical data (see below) show is that even short-range additional interactions induce a first-order transition with a rather robust supercooled liquid phase surviving below the melting temperature. In order to characterize the hyperloop corrections to the liquids phase, we looked to the smallest hyperloop for the model defined at the beginning of this section. In order to do this we used a simulated annealing method, explained in detail in Appendix A 2. According to simulated annealing, the smallest hyperloop of the high-temperature series is the one shown in Fig. 3, which is made of 54 plaquettes from $H_{\rm TPM}$ and 10 plaquettes from $H_{\rm extra}$. Even if such hyperloop is "big," in the sense that it provides a correction of the order $[\tanh(\beta)]^{64}$ to the high-temperature expansion of the free energy, it contains a number of plaquettes from the additional sublattice (10 plaquettes) well below the threshold of $(m^*+1)^2 = 49$ plaquettes (from the additional sublattice) discussed above in this paragraph.

The next question can then be, what about if we add to the TPM Hamiltonian not all the plaquettes of the sublattice but just a fraction of them randomly chosen? That is, what about if the sums in Eq. (12) run over the plaquettes of a special instance of the disorder, which corresponds to have in $H_{\rm extra}$ just a fraction c of the plaquette of the regular sublattice? The answer is that hyperloops will still be there, just in a smaller amount compared to having all the plaquettes of the regular sublattice. Let us consider for instance the hyperloop of Fig. 3, made of 10 close-by plaquettes of the regular sublattice and 54

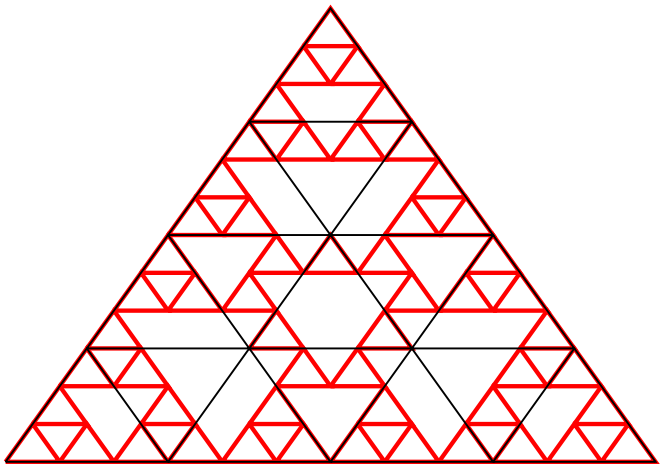

FIG. 3. Smallest hyperloop of the high-temperature expansion for the modified TPM with extra short-range plaquettes discussed in Sec. II B. In the figure can be counted 54 small plaquettes of the original TPM lattice (thick red triangles) and 10 plaquettes of the auxiliary sublattice (thin black triangles), which has as elementary cells equilateral triangles of side 3.

plaquettes of the TPM. For a random choice of the additional plaquettes such that a fraction c of the total number present in the sublattice is taken, in a high-temperature expansion like the one in Eq. (16) a contribution as $M_L[\tanh(\beta)]^{64}$ is replaced by $cM_L[\tanh(\beta)]^{64}$, and correspondingly the correction to the partition function becomes $\exp\{c\alpha_L N[\tanh(\beta)]^{64}\}$.

The difference between adding randomly chosen long-range and short-range plaquettes is at this point clear: while in the former case it can be proved that the high-temperature expansion is trivial and there is an entropic crisis, in the latter case there are corrections coming from finite hyperloops, and these corrections are most likely preventing any entropic crisis. For this case we present the numerical evidence that, even with no clue on the presence of an entropic crisis, the idea to add interactions to the TPM is a good strategy to induce a nontrivial thermodynamics characterized by the presence of a supercooled liquid phase.

Numerical simulations. In order to provide the numerical evidence that even short-range interactions produce a nontrivial thermodynamics we considered the case of a random choice of the plaquettes on the regular sublattice and we found it convenient also to put weaker interactions on these additional plaquettes. Actually we considered the Hamiltonian $H_{\rm extra} = -J_1\sum_{a=1}^{M_L}\sigma_{i_a}\sigma_{j_a}\sigma_{k_a}$, with $J_1 = 1/5$ and with the sum running on a finite fraction of the sublattice plaquettes. On one hand the random choice of a subset of the plaquettes on the regular sublattice decreases the number of finite hyperloops in the high-temperature expansion; on the other hand a reduced strength of interactions on these plaquettes decreases the weight of these hyperloops. Monte Carlo simulations done with $J_1 = 1$ showed that also with short-range plaquettes there is a melting temperature T_m, but differently from the case of long-range plaquettes (with a random choice of the spins) the system decays to the ordered ground state as soon as $T < T_m$. Data are not reported here, but we found that with the same annealing protocol used for long-range plaquettes, namely

temperature jumps of $\Delta T = 0.04$ each 10^6 or 10^7 Monte Carlo steps (depending on the temperature), the system reaches the equilibrium ground states for all temperatures $T < T_m$ with $M_L = 0.1N$ additional short-range plaquettes. Before commenting on the numerical data obtained with $J_1 = 1/5$, let us notice that when the additional plaquettes are taken from a regular sublattice, even for $T > T_m$ the high-temperature expansion yields a small but finite magnetization. This can be clearly seen looking at the high-temperature expansion of the magnetization:

$$\begin{aligned}
&\frac{1}{N}\left\langle \sum_{i=1}^{N} \sigma_i \right\rangle \\
&= \frac{1}{N\mathcal{Z}} \sum_{i=1}^{N} \sum_{\boldsymbol{\sigma}} \sigma_i e^{-\beta(H_{\mathrm{TPM}}[\boldsymbol{\sigma}]+H_{\mathrm{extra}}[\boldsymbol{\sigma}])} \\
&= \frac{[\cosh(\beta)]^{M_L}}{N\mathcal{Z}} \left[\sum_{i=1}^{N} \sum_{r=1}^{M_L} \langle \sigma_i \sigma_{r_i} \sigma_{r_j} \sigma_{r_k} \rangle_{\mathrm{TPM}} \tanh(J_1\beta) + \cdots \right] \\
&= \frac{M_L}{N} \tanh^6(\beta) \tanh(J_1\beta) + \cdots , \qquad (19)
\end{aligned}$$

which, as can be seen in Fig. 4, nicely compares with the results of numerical simulations. As is clear from Eq. (19), the first effect of taking $J_1 < 1$ is to reduce the high-temperature magnetization in the vicinity of T_m making the supercooled liquid phase more stable. Let us briefly explain how the equalities in Eq. (19) are obtained. From the first to the second line of Eq. (19) we just wrote down explicitly the high-temperature expansion. The last identity of Eq. (19) is clear if one recalls that each plaquette of H_{extra} is represented by a triplets of spins $\sigma_{r_i}\sigma_{r_j}\sigma_{r_k}$ at the vertices of an equilateral triangle of side 3. It can be easily realized that those spins form a *hyperfield* [25] when multiplied with the plaquettes of H_{TPM} which are enclosed within the perimeter of the same triangle. Borrowing the terminology of [25] we call a *hyperfield* a set of interactions such that all spins but one, σ_i, appear an even number of times. Since the plaquettes of H_{extra} are all represented by triplets of spins placed at the corners of equilateral triangles of side 3, each of them contributes a hyperfield σ_i in the high-temperature expansion, and this hyperfield becomes a hyperloop of weight $[\tanh(\beta)]^6 \tanh(J_1\beta)$ when multiplied for the corresponding spin σ_i appearing in the definition of the magnetization. Then, by taking also the approximation $\mathcal{Z} \sim 2^N[\cosh(\beta)]^{N+M_L}$ (which is exact in the case of long-range plaquettes; see Sec. II A), we have the result of the last line in Eq. (19).

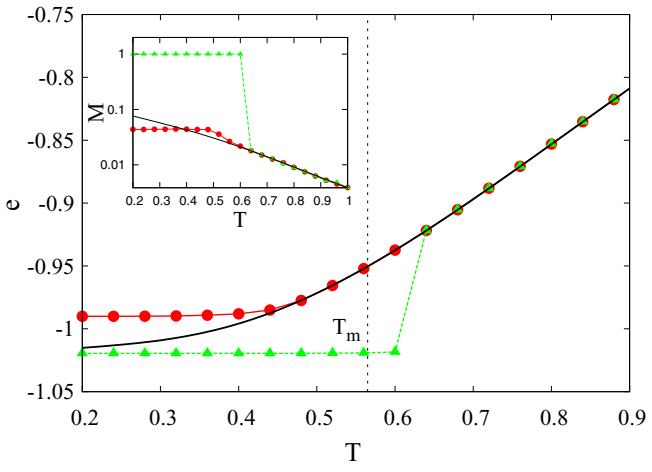

FIG. 4. Main: Energy hysteresis cycle for a TPM model with additional short-range plaquettes. We simulated the model on a lattice with the shape of a rhombus (see for instance the representation of Fig. 2) with $L = 128$ plaquettes per side and a concentration of additional plaquettes $\alpha_L = 0.1$: the coupling coefficient of the additional plaquettes is $J_1 = 1/5$. Red circles: Cooling (cooling rate from 10^6 to 10^7 Monte Carlo steps per $\Delta T = 0.04$). Green triangles: Heating. Continuous black line: High-temperature expansion, $e(T) = -[\alpha_L \tanh(J_1/T) + \tanh(1/T)]$. Inset: Magnetization hysteresis cycle for the same model with the same cooling/heating protocol. Red circles: Cooling. Green triangles: Heating. Continuous line: $m(T)$ from the high-temperature expansion: $m(T) = \alpha_L[\tanh(1/T)]^6 \tanh(J_1/T)$, with $\alpha_L = 0.1$ and $J_1 = 1/5$.

Our numerical study showed that for the smaller value of the coupling constant $J_1 = 1/5$, a number $M_L = 0.1N$ of additional plaquettes, and the same annealing protocol already mentioned above in this section, at all the temperatures studied the system does not decay to the ordered ground state; see Fig. 4. In the inset of Fig. 4 is shown the behavior of the magnetization, which in the paramagnetic phase is well reproduced by the high-temperature expansion. The model with randomly chosen plaquettes on a regular sublattice seems therefore a good one to reproduce the standard scenario of realistic glass formers: a first-order phase transition to an ordered ground state plus a long-lived supercooled liquid phase. A system where a similar behavior is found is the coupled two-level system (CTLS) model [29,30]. The CTLS is a nondisordered plaquette model which presents, as our TPM with additional plaquettes, a first-order transition to an ordered ground state and a metastable supercooled liquid phase. To summarize, we can say that even when is not possible to argue about the existence of a thermodynamic glass transition, the addition of short-range plaquettes to the TPM induces a first-order phase transition and the formation of a robust supercooled liquid phase. We can therefore argue that even with short-range interactions the presence of a nontrivial thermodynamics is controlled by the ratio $\alpha = M/N$ between the number of plaquettes and the number of spins. In plaquette models with short-range interactions the glass-forming ability is then a matter of competition between two time scales: the time scale to nucleate the the crystal and the relaxation time of the supercooled liquid. For a detailed discussion on how a stable supercooled liquid phase can be obtained by appropriately tuning the cooling rate procedure let us refer the reader to [24,29,30].

III. RANDOM-DILUTED TPM: PHASE DIAGRAM AT $T = 0$

The analysis of the present section is based on the deep connection between the thermodynamics of plaquette models and the properties of solutions of the XOR-SAT problem. The latter is a constraint satisfaction problem which has been very successfully described within the landscape scenario of the ideal glass transition [21]. The relation between the TPM and the XOR-SAT comes from the fact that the ground states of

a TPM can be obtained as the solutions of a XOR-SAT. By assuming the change of variables $\sigma_i = (-1)^{n_i}$, a ground state of the TPM can be always written as the solution of the system of linear equations:

$$\left(\sum_{i\in\partial p} n_i\right)_{\mathrm{mod}2} = 0, \qquad \forall p, \tag{20}$$

where with the notation $i \in \partial p$ we indicate the spins in the plaquette p. The ground states of the TPM are represented by all the solutions of the system in Eq. (20), which is made of M linear equations, the plaquettes, in N variables, the spins. The topology of the interaction network is specified by the equations of the linear system. For instance, in the triangular 2D lattice of the TPM each spin n_i appears in three equations and in each equation it is coupled to the two other spins belonging to the same plaquette. When the network formed by spins and plaquettes corresponds to a random hyper-graph [which is a locally treelike network with loops of order $\ln(N)$] it is known that the properties of the solutions of the XOR-SAT are fully determined by the parameter $\alpha = M/N$ [21]. For a TPM on the random graph, even with nondisordered interactions [23], two transitions are found varying α, respectively at α_d and α_{unsat}. When $\alpha < \alpha_d$ the system of equations in Eq. (20) is solvable and it happens that a few spins flips are sufficient to go from one solution to another; the set of solutions forms a unique cluster. On the contrary, when $\alpha_d < \alpha < \alpha_{\mathrm{unsat}}$ the set of solutions splits in clusters separated by extensive barriers; it is necessary to flip an extensive number of spins to pass from one cluster to the other. Finally, when $\alpha > \alpha_{\mathrm{unsat}}$ the system in Eq. (20) is no longer solvable: at α_{unsat} the SAT/UNSAT transition takes place. With respect to any random update algorithm designed to move across the phase space of variables $\{n_i\}_{i=1,\ldots,N}$, the SAT/UNSAT transition represents an ideal glass transition. The nonsatisfiable phase of the XOR-SAT coincides with the glass phase of the related TPM: as a consequence, when $\alpha > \alpha_{\mathrm{unsat}}$ the TPM (on random graph) is in the glass phase at $T = 0$, which means that it has an ideal glass transition at $T > 0$.

A. Leaf-removal algorithm and $T = 0$ phase diagram

The "leaf-removal" algorithm is a decimation scheme used to study the satisfiability of the XOR-SAT model on random regular graphs [21]. We discuss here how this algorithm can be used to investigate the properties of our random-diluted TPM. A "leaf" is every spin which appears in only one plaquette (i.e., every variable appearing in a single equation of the XOR-SAT problem); "leaf removal" is a prescription to remove iteratively from the graph all the spins which are (or become) leaves. The procedure is iterative because after the removal of each leaf new leaves may appear in the system. When $\alpha < \alpha_d$ leaf removal is able to remove all the spins from the graph, while for $\alpha > \alpha_d$ the algorithm stops leaving the so called "core," i.e., a set of spins among which no one is a leaf. The clustering of solutions of the XOR-SAT at α_d corresponds to the formation of the core. The SAT/UNSAT transition takes place when the number of equations (plaquettes) in the core, M_c, becomes larger than the number of variables left on it, N_c. The critical value α_{unsat} can be determined by studying the ratio $M_c/N_c = \alpha_c$ in the core, and corresponds to $\alpha_c = 1$. On a random regular graph the dependence of M_c and N_c on α can be determined analytically in the thermodynamic limit [21]. The leaf-removal algorithm can be used to study the formation of the core and the behavior of α_c on the core for a XOR-SAT on every kind of topology. Nevertheless, only for random graphs is it proven that the formation of the core corresponds to the clustering transition and the value $\alpha_c = 1$ to the SAT/UNSAT transition [21]. On finite-dimensional topologies a proof of this correspondence is still lacking. This notwithstanding, we studied numerically the action of the leaf removal on our random-diluted TPM, proposing a "tentative" phase diagram. We compare this numerical phase diagram with that obtained by analytically solving leaf removal for the representation of our random-diluted TPM on the random graph; in this case the leaf-removal analysis yields exactly the thermodynamic properties of the system [21]. Let us stress that by running the leaf-removal algorithm in a finite-dimensional geometry, we may find both a critical value α^* for the formation of the core and a critical value α^{**} where $M_c/N_c = 1$, but there is no proof that they correspond respectively to the clustering and UNSAT transition. This is the reason why the phase diagram of Fig. 5 is just tentative. The conjecture that even in finite dimensions at α^{**} the UNSAT transition really takes place, namely $\alpha^{**} = \alpha_{\mathrm{unsat}}$, is supported within our analysis just by the agreement that we find between the numerical finite-dimensional and exact mean-field predictions on the phase diagram.

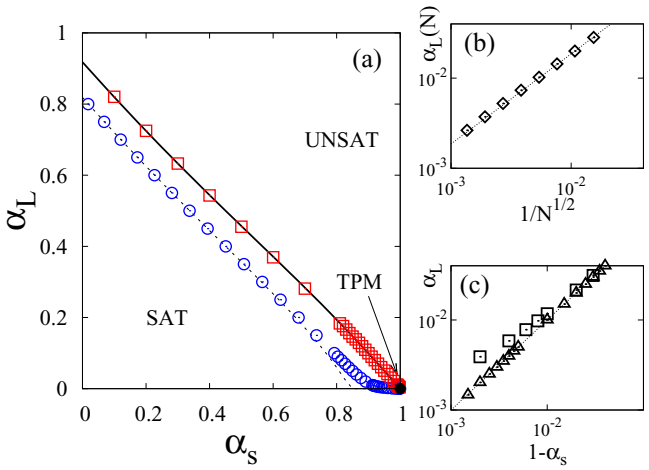

FIG. 5. Panel (a): $T = 0$ phase diagram of the random-diluted TPM [see Eq. (23)]. Symbols represent numerical data obtained running the leaf-removal algorithm on finite-dimensional geometries, lines the results of analytical calculation on the Bethe lattice. Circles (blue) and the dotted line represent the critical line for the formation of the core, squares (red) and the continuous line are the critical line for the SAT/UNSAT transition. Panel (b): Diamonds, numerical estimate in finite dimensions of the critical value α_L for the SAT/UNSAT transition as function of $\sqrt{N}$, with N the size of the system, at fixed $\alpha_s = 1$; dotted line, linear fit of data. Panel (c): Zoom of the SAT/UNSAT transition line close to the point ($\alpha_s = 1, \alpha_L = 0$). Triangles, analytic result on the random graph; squares, numerical data for a system with $N = 10^6$ spins; dotted line, linear fit of analytic prediction.

Until now we have discussed a single parameter α, but for the random-diluted TPM and its representation on the random graph we need two: α_s, which represents the concentrations of plaquettes in the 2D lattice, and α_L, which represents the concentration of long-range plaquettes. The random-diluted TPM corresponds in practice to a random-graph structure, parametrized by α_L, built on the top of a diluted two-dimensional network, characterized by a dilution parameter α_s. The probability that a spin is attached to ℓ short-range plaquettes depends on α_s and is

$$\rho_\ell(\alpha_s) = \binom{3}{\ell}\alpha_s^\ell(1-\alpha_s)^{3-\ell}, \tag{21}$$

while the probability that a spin is attached to ℓ long-range plaquettes depends on α_L and reads

$$p_\ell(\alpha_L) = e^{-3\alpha_L}\frac{(3\alpha_L)^\ell}{\ell!}. \tag{22}$$

The probability that a spin is attached to overall ℓ plaquettes is

$$n_\ell = \mathcal{N}^{-1}\sum_{r=0}^{\ell_0}\rho_r(\alpha_s)p_{\ell-r}(\alpha_L), \tag{23}$$

with

$$\begin{aligned}\mathcal{N} &= \sum_{\ell=0}^{\infty}\sum_{r=0}^{\ell_0}\rho_r(\alpha_s)p_{\ell-r}(\alpha_L)\\ &= 1-\sum_{r=0}^{3}\sum_{k=r}^{3}\rho_r(\alpha_s)p_{k-r}(\alpha_L)+\sum_{k=0}^{3}\sum_{r=0}^{k}\rho_r(\alpha_s)p_{k-r}(\alpha_L),\end{aligned} \tag{24}$$

where $\ell_0 = \min\{\ell,3\}$. When the random-diluted TPM is represented on the random graph the small-world topology, i.e., the two-dimensional lattice plus a few long-range connections, is lost. The only ingredient of the original model which is kept is the presence of two kinds of plaquettes, each characterized by a different probability for the connectivity with the spins. For the representation on the random graph the adjectives "short-range" and "long-range" are therefore only conventional: the former denotes the plaquettes attached to spins with the probability of Eq. (21), the latter plaquettes attached to spins with the probability of Eq. (22).

Figure 5 shows the phase diagram of the random-diluted TPM obtained by running the leaf-removal algorithm in finite dimensions and that obtained by solving the corresponding equations (see Appendix B) in the mean-field (random-graph) approximation. In both cases we determine a "critical" line $(\alpha_s^{\rm core},\alpha_L^{\rm core})$ for the formation of the core (clustering transition on the random graph) and a critical line $(\alpha_s^{\rm unsat},\alpha_L^{\rm unsat})$ from the condition $M_c/N_c = 1$ (UNSAT transition on random graph). First of all, let us note the agreement between numerical and analytical predictions on the location of the line $(\alpha_s^{\rm unsat},\alpha_L^{\rm unsat})$ in Fig. 5. Since with $\alpha_s = 0$ the random-diluted TPM is perfectly equivalent to the XOR-SAT [21], for $\alpha_s = 0$ we recover the random-graph result $\alpha_L^{\rm unsat} = 0.918$ [21]. By looking at the left part of the phase diagram in Fig. 5 we are indeed not surprised that for $\alpha_L \sim 1$ and $\alpha_s \ll 1$ the analytic predictions on the random graph are in agreement with the numerical analysis in finite dimensions: the random-diluted TPM is almost a random graph for these values of the parameters. What is more surprising is to find an agreement between the numerical and the analytical estimate of $(\alpha_s^{\rm unsat},\alpha_L^{\rm unsat})$ in the bottom right part of the phase diagram in Fig. 5, where $\alpha_L \ll 1$ and $\alpha_s \sim 1$. In this region the random-diluted TPM is almost a two-dimensional model, while the analytical predictions are given for a random-graph geometry. It really appears that as soon as a few long-range interactions are added to the TPM its physics becomes immediately well represented by the random graph. If the true thermodynamics of the random-diluted TPM could be predicted on the basis of the analytic results of Fig. 5, we would say that as soon as any finite concentration α_L of random plaquettes is added to the TPM the model develops a finite-temperature glass transition. We do not still have a proof of that; therefore by now this is just a conjecture supported by the agreement between numerics and analytics on the location of the $(\alpha_s^{\rm unsat},\alpha_L^{\rm unsat})$ line. The small panels of Fig. 5 illustrate the finite-size scaling analysis needed to assess the agreement of analytical and numerical predictions on the behavior of the $(\alpha_s^{\rm unsat},\alpha_L^{\rm unsat})$ transition line close to the point $(\alpha_s = 1,\alpha_L = 0)$.

Concerning the analytical and numerical data on the location of the $(\alpha_s^{\rm core},\alpha_L^{\rm core})$ line in the bottom right part of the phase diagram of Fig. 5 we find a certain disagreement: two main comments on this are in order. First, it is well known that the clustering transition which takes place at α_d on the random graph, and which corresponds to dynamical ergodicity breaking, is a purely mean-field phenomenon which turns into a crossover in finite dimensions. From this point of view we are not concerned about the disagreement found between the analytical (mean-field) and numerical (finite-dimensional) results on the position of the line $(\alpha_s^{\rm core},\alpha_L^{\rm core})$. On the other hand, the numerical results on the location of the line $(\alpha_s^{\rm core},\alpha_L^{\rm core})$ are *per se* interesting and represent a useful source of information on the model, as will be discussed in the next section, Sec. III B.

B. Leaf removal and exact calculation of $\mathcal{Z}$

The numerical estimate of the position of the line $(\alpha_s^{\rm core},\alpha_L^{\rm core})$ in the phase diagram of Fig. 5 is quite interesting even in the case of a finite-dimensional geometry. In this case the line $(\alpha_s^{\rm core},\alpha_L^{\rm core})$ is the upper boundary of the region where the partition function of the random-diluted TPM can be exactly calculated and has the expression

$$\mathcal{Z} = 2^N[\cosh(\beta)]^{M_s+M_L} = (2[\cosh(\beta)]^{\alpha_s+\alpha_L})^N. \tag{25}$$

The exact explanation of why leaf removal allows us to check whether or not the partition function can be exactly summed, yielding the expression in Eq. (25), can be found in Appendix C. The behavior of the $(\alpha_s^{\rm core},\alpha_L^{\rm core})$ line (numerical data) close to the point $(\alpha_s = 1,\alpha_L = 0)$ in the phase diagram of Fig. 5, which correspond also to the data in the main panel of Fig. 6, shows that, among all the two-dimensional models belonging to the line $(\alpha_s,0)$, the only one such that any concentration $\alpha_L > 0$ of long-range plaquettes is "critical" is the original TPM. As "critical" we mean that the possibility to exactly compute $\mathcal{Z}$ according to the expression in Eq. (25) is spoiled as soon as any finite concentration of long-range

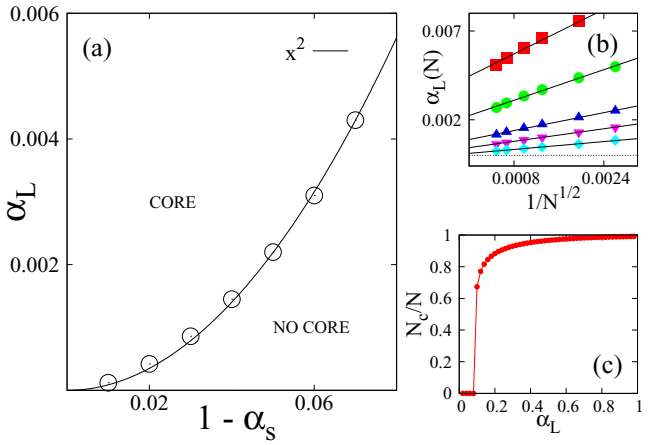

FIG. 6. Panel (a): Circles are the critical values (α_s,α_L) for the formation of the core extrapolated in the thermodynamic limit from numerical data at finite N. The continuous line represents a quadratic fit of data $y = ax^2$, with prefactor $a = 0.877$; see also Eq. (26) in Sec. III B. Panel (b): Critical values $\alpha_L(N)$ for core formation as a function of the size N of the system for different values of α_s (different symbols), from top to bottom: $\alpha_s = 0.93,0.95,0.97,0.98,0.99$. Panel (c): Concentration of spins in the core as a function of α_L for a fixed value of $\alpha_s = 0.8$, with $N = 1024^2$.

plaquettes, $\alpha_L > 0$, is introduced. In order to make ourselves really sure about that we need to know the behavior of the system in the thermodynamic limit. In the top right panel of Fig. 6 is presented the study of finite-size effects, while in the main panel of Fig. 6 appears the resulting estimate for some points of the line $(\alpha_s^{\rm core},\alpha_L^{\rm core})$. These point can be well interpolated with a parabola:

$$\alpha_L^{\rm core} + O(N^{-1/2}) \sim \left(1 - \alpha_s^{\rm core}\right)^2. \tag{26}$$

The parabolic fit of the data in the main panel of Fig. 6 represents the main evidence that the only model on the line $(\alpha_s,\alpha_L = 0)$ such that the addition of extra plaquettes is critical is the TPM model. To conclude this section let us notice that also in an almost finite-dimensional geometry, $\alpha_s = 0.8$ and $\alpha_L \sim 1$, we find that the formation of the core is a discontinuous process, see panel (c) of Fig. 6, as is usually found for random geometries. This result supports the view that the physical properties of the random-diluted TPM can be well represented even on a random graph. Our finding that the formation of the core happens discontinuously upon changing α_L also in finite dimensions is intriguing: it is not the first time that a similar discontinuous transition has been observed in finite dimensions [32–36]. The spiral model of [33,34], which is a KCM, is the example of a finite-dimensional system where a dynamical transition really takes place and is due to the formation in the system of an infinite compact cluster of "frozen" (i.e., not allowed to move due to the kinetic constraint) spins. A cluster of spins which cannot flip due to a kinetic constraint is not exactly reducible to the leaf-removal "core" of our random-diluted TPM. Yet, if the mean-field scenario is predictive also for the behavior in finite dimensions, the formation of the core should take place when, in order to move in phase space, we need to flip an extensive number of spins, which we may very roughly think about as a "frozen cluster."

IV. RANDOM-DILUTED TPM ON RANDOM GRAPH: PHASE DIAGRAM AT $T > 0$

In this section we present results on the finite-temperature phase diagram of the random-diluted TPM model on the random regular graph (Bethe lattice), where the temperature T_K of the ideal glass transition can be computed exactly.

According to the presence of both long- and short-range plaquettes in the random-diluted TPM, the cavity equations (Appendix D) for its representation on the random graph are written by means of two different cavity fields, as is usually done for small-world networks [31]. The field $u_{\alpha\to i}$ determines the probability distribution $p(\sigma_i) \sim e^{u_{\alpha\to i}\sigma_i}$ when all the plaquettes attached to σ_i but α are removed, and α is a long-range plaquette. The field $v_{\alpha\to i}$ determines the probability distribution $p(\sigma_i) \sim e^{v_{\alpha\to i}\sigma_i}$ when all the plaquettes attached to σ_i but α are removed, and α is a short-range plaquette. The cavity equations, written and discussed in Appendix D, allow us to find the equilibrium values of the fields u and v, from which all the thermodynamic potentials can be calculated (formulas are in Appendix D). For fixed values of α_s and α_L, the glass transition temperature T_K is obtained as the temperature where the configurational entropy Σ vanishes. In Fig. 7 is represented the phase diagram of the random-diluted TPM in the plane (α_L,T) for two values of the short-range plaquette concentration: $\alpha_s = 1$ and $\alpha_s = 0.96$. While for $\alpha_s = 1$ the glass transition temperature vanishes when also the concentration α_L of long-range plaquettes vanishes, when $\alpha_s = 0.96$ we find that T_K vanishes at a finite value of the additional plaquette concentration, $\alpha_L^{\rm min} > 0$; when α_L belongs to the interval $[0,\alpha_L^{\rm min}]$ the system is liquid at all the temperatures. By definition, the finite-temperature phase diagram of the random-diluted TPM on the Bethe lattice must agree with the analytical solution of the leaf-removal algorithm, which is also obtained on the random graph. From the leaf-removal analysis of Sec. III we already know that for all the concentrations of short-range plaquettes $\alpha_s < 1$ there is always a value $\alpha_L^{\rm min} > 0$ such that for concentrations of

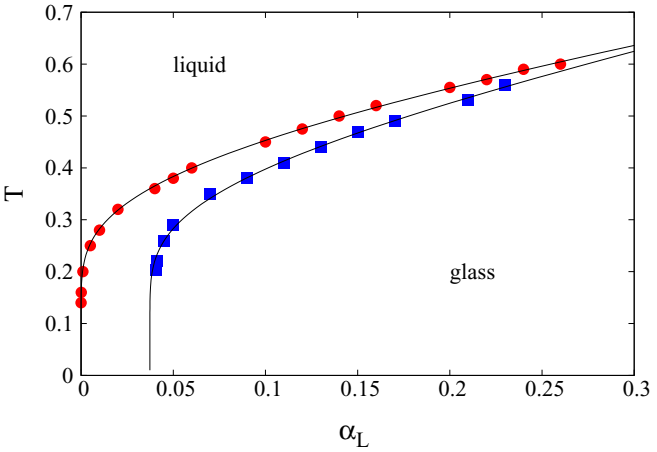

FIG. 7. Phase diagram of the random-diluted TPM model on the Bethe lattice in the (α_L,T) plane for two different values of dilution α_s: circles (red), $\alpha_s = 1$; squares (blue), $\alpha_s = 0.96$; continuous lines, fits of the data with the function $\alpha_L(T) = C_1\exp(-C_2/T) + \alpha_L(0)$, where C_1 and C_2 are fit parameters.

long-range plaquettes $\alpha_L < \alpha_L^{\min}$ the system is liquid at all temperatures. This happens because, as we discussed in Sec. III (see also Fig. 5), the only value of α_s such that the related XOR-SAT problem becomes UNSAT (glass phase) for every $\alpha_L > 0$ is just $\alpha_s = 1$. Let us note that the phase diagram of our model in the plane (α_L, T), i.e., for a fixed concentration α_s of short-range plaquettes (see Fig. 7), has a remarkable similarity to the phase diagram in the plane (ϵ, T) of [19], where ϵ is an external field coupling different replicas of a TPM. According to [19] the critical line $T_K(\epsilon)$ approaches the origin with infinite slope [19], $T_K \sim [\ln(\epsilon)]^{-1}$; we are going to show that the same happens in our case to $T_K(\alpha_L)$, when the concentration α_L of long-range plaquettes is sent to zero. We want to emphasize that α_L plays a role analogous to ϵ. The argument for the behavior of $T_K(\alpha_L)$ in our system is rather simple and is exact on the random graph. From [21] we know that in the UNSAT phase the ground states of a TPM on a random graph have extensive energy. The energy of the system is by definition the sum over plaquette energies, so that when a ground state has extensive energy it means that there is an extensive amount of excited plaquettes in it. To have ground states with extensive energy is equivalent to having a minimum value, $\varepsilon^{\min}$, for the energy per plaquette. In the TPM the concentration of defects at low temperatures behaves as $c \sim e^{-2\beta}$ and we can assume that in the presence of a small number of extra plaquettes this dependence is roughly the same, say $c \sim e^{-a2\beta}$ with $a \sim 1$. Since the existence of a minimum value $\varepsilon^{\min}$ is equivalent to a minimum concentration of excited plaquettes, also a minimum $c^{\min}$ is fixed. From the constraint of a minimum allowed concentration of excited plaquettes we can define a critical temperature T_K as $c^{\min} = e^{-a2/T_K}$. Clearly the minimum value of the energy per plaquette and the minimum concentration of excited plaquettes must be proportional $c^{\min} \sim \varepsilon^{\min}$. By looking at the behavior of the energy in the ground states as a function of α presented in [21], it is reasonable to assume also for our random-diluted TPM on random graph that we have $\varepsilon^{\min} \sim \alpha_L^b$, with $b \sim 1$. Putting together all the information collected above we can conclude that $\alpha_L^b = e^{-a2/T_K}$, which in turn implies

$$T_K = -\frac{a}{b}\frac{2}{\ln(\alpha_L)}. \tag{27}$$

Equation (27) allows us a good fit of the data in Fig. 7 and accounts for the infinite slope of the curve $T_K(\alpha_L)$ approaching $\alpha_L = 0$. This infinite slope is signaling that around $\alpha_L = 0$ the random-diluted TPM is sensitive to arbitrarily small perturbations, which induce the formation of the glass phase. The same happens for the original two-dimensional triangular plaquette model in the presence of an external field ϵ coupling replicas [19].

V. CONCLUSIONS

In this paper we studied the thermodynamic properties of the triangular plaquette model in the presence of additional plaquettes; namely we looked to what happens when $\alpha = M/N > 1$, where M is the number of plaquettes and N the number of spins. We have demonstrated that in the small-world lattice obtained by adding long-range plaquettes to the TPM the high-temperature expansion of the free energy, which can be computed in the annealed approximation, has an entropic crisis. In the same model we find the numerical evidence of a first-order transition to a an ordered phase at T_m, with a remarkably stable supercooled liquid phase at lower temperatures. The same phenomenology is found also when the additional interactions are short range, although in this case there are corrections to the high-temperature expansion which very likely prevent the entropy crisis. Since the presence of an ideal glass transition is more likely when the entropy crisis takes place, we studied in more detail in the rest of the paper the model with long-range additional plaquettes, i.e., the random-diluted TPM. Our deepest investigation of the thermodynamic properties of the random-diluted TPM was carried on by means of the leaf-removal algorithm, usually applied to constraint satisfaction problems [21]. The advantage of leaf removal is that it allows us to infer the thermodynamic properties of the model just analyzing the interaction network. The drawback is that the correspondence between the properties of the interaction network and the thermodynamics is exact only for random geometries. By means of the leaf-removal algorithm we obtained a tentative phase diagram in the space of parameters (α_s, α_L), where α_s is the concentration of plaquettes in the 2D triangular lattice while α_L is the concentration of "long-range" plaquettes. Such a phase diagram suggests that among the 2D plaquette models with different dilutions α_s the original TPM [15] ($\alpha_s = 1$) is the only one where the addition of any concentration of long-range plaquettes makes the thermodynamic nontrivial. That is why we say that the TPM is stochastically *unstable*: arbitrarily small perturbations of the Hamiltonian have dramatic effects on the thermodynamic properties of the model. Moreover, our results suggest that even in finite dimensions the parameter that controls this *stochastic instability* is the ratio α between the number of plaquettes and the number of spins. These considerations are also compatible with the results of [19,20]. In [19,20] is shown how the TPM supports both dynamic and thermodynamic phase transition under the influence of arbitrarily small external fields. We find remarkable the similarity between the behavior of the glass transition temperature T_K as function of α_L in our random-diluted TPM (on the random graph) and as function of ϵ in [19]: in both situations an infinitesimal amount of perturbation lifts the critical temperature T_K to finite values. We can conclude by saying that further investigations on the stochastic stability of the TPM are mandatory.

ACKNOWLEDGMENTS

We thank J.-P. Garrahan, F. Ricci-Tersenghi, and R. Santachiara for useful discussions. G.G. acknowledges support from the project NSTGEA of Labex PALM.

APPENDIX A: HIGH-TEMPERATURE EXPANSION WITH ADDITIONAL PLAQUETTES

1. Random choice of spins in the new plaquettes: Random-diluted TPM

(a) Triviality of the high-temperature expansion

In order to say that the high-temperature expansion of Eq. (6) in Sec. II A is trivial we need to show that

$$\lim_{N\to\infty} \binom{M_L}{m} \langle \tau_1 \dots \tau_m \rangle_{\text{TPM}} = 0, \qquad \forall m. \tag{A1}$$

Let us recall that the correlation function in Eq. (A1) is the multispin correlation function $\langle\sigma_1 \dots \sigma_{3m}\rangle_{\rm TPM}$, where the $3m$ spins are randomly chosen with uniform probability on the 2D lattice. The multispin correlation function $\langle\sigma_1 \dots \sigma_{3m}\rangle_{\rm TPM}$ is different from zero only when it is possible to find plaquettes in the TPM such that a set of one or more hyperloops can be formed which include all the $3m$ spins. Since in the TPM we know that both the magnetization $\langle\sigma_i\rangle_{\rm TPM} = 0$ and the two-spin correlation function $\langle\sigma_i\sigma_j\rangle_{\rm TPM} = 0$ are zero, each of the hyperloops contains necessarily at least three spins. At the same time, since the $3m$ spins are chosen with uniform probability on the lattice, the typical distance between any two of them is $O(\sqrt{N})$. This in turn means that the typical distance between any two spins which belong to the same hyperloop is also $O(\sqrt{N})$. Then, due to the fact that we consider the thermodynamic limit at fixed m, any hyperloop which contains the $3m$ spins of the the additional plaquettes contains also an infinite number of plaquettes of the TPM model. More precisely, since the hyperloop connects spins at a distance $O(\sqrt{N})$, the number of plaquettes of the TPM in the hyperloop is $O(N^{d_{\rm H}/2})$, where d_H is the fractal dimension of the Sierpinski gasket in $D = 2$. One then has that the value of the correlation function between $3m$ spins chosen with uniform probability on the lattice is dominated at large N by the weight of the hyperloop which connects all the spins: $\langle\tau_1 \dots \tau_m\rangle_{\rm TPM} \sim [\tanh(\beta)]^{N^{d_{\rm H}/2}}$. We can therefore conclude by noticing that for every m one has

$$\lim_{N\to\infty} \binom{M_L}{m} \langle\tau_1 \dots \tau_m\rangle_{\rm TPM} \sim N^m [\tanh(\beta)]^{N^{d_{\rm H}/2}} = 0. \quad \text{(A2)}$$

(b) *Estimate of* $\overline{\mathcal{Z}^2}$

Making use of the argument discussed in Appendix A 1 a, we show here that the partition function of the modified TPM of Sec. II A is self-averaging, namely that we have $\overline{\mathcal{Z}}^2 = \overline{\mathcal{Z}^2}$. Let us first write the expression of the high-temperature series of $\mathcal{Z}^2$ in a convenient way and then take the average over the disorder. We have that, for a given instance of the disorder, $\mathcal{Z}^2$ reads as

$$\begin{aligned}\mathcal{Z}^2 &= \sum_{\boldsymbol{\sigma},\mathbf{s}} e^{-\beta H_{\rm TPM}[\boldsymbol{\sigma}]-\beta H_{\rm TPM}[\mathbf{s}]+\beta\sum_{r=1}^{M_L}\sigma_{i(r)}\sigma_{j(r)}\sigma_{k(r)}+s_{i(r)}s_{j(r)}s_{k(r)}} \\ &= 2^{2N}[\cosh(\beta)]^{2M_L+2N}\Big\langle\prod_r\{1+\tanh(\beta)[\sigma_{i(r)}\sigma_{j(r)}\sigma_{k(r)} \\ &\quad +s_{i(r)}s_{j(r)}s_{k(r)}]+\tanh(\beta)^2 \\ &\quad \times[\sigma_{i(r)}\sigma_{j(r)}\sigma_{k(r)}s_{i(r)}s_{j(r)}s_{k(r)}]\}\Big\rangle_{\boldsymbol{\sigma},\mathbf{s}} \end{aligned} \quad \text{(A3)}$$

where we have introduced the average:

$$\langle\,\rangle_{\boldsymbol{\sigma},\mathbf{s}} = \mathcal{Z}_{\rm TPM}^{-2}\sum_{\boldsymbol{\sigma},\mathbf{s}} e^{-\beta(H_{\rm TPM}[\boldsymbol{\sigma}]+H_{\rm TPM}[\mathbf{s}])}. \quad \text{(A4)}$$

It is then useful for what follows to define also

$$\begin{aligned}\langle\,\rangle_{\boldsymbol{\sigma}} &= \mathcal{Z}_{\rm TPM}^{-1}\sum_{\boldsymbol{\sigma}} e^{-\beta H_{\rm TPM}[\boldsymbol{\sigma}]}, \\ \langle\,\rangle_{\mathbf{s}} &= \mathcal{Z}_{\rm TPM}^{-1}\sum_{\mathbf{s}} e^{-\beta H_{\rm TPM}[\mathbf{s}]}. \end{aligned} \quad \text{(A5)}$$

Now, in order to lighten the notation, it is worthwhile to use the plaquette variables $\tau_r = \sigma_{i(r)}\sigma_{j(r)}\sigma_{k(r)}$ and $t_r = s_{i(r)}s_{j(r)}s_{k(r)}$ and use the symbol g_r to represent the polynomial expression in Eq. (A3) corresponding to the plaquette r,

$$g_r = \tanh(\beta)[\tau_r + t_r] + \tanh(\beta)^2\tau_r\sigma_r, \quad \text{(A6)}$$

so that we can write the high-temperature series of $\mathcal{Z}^2$ as

$$2^{2N}[\cosh(\beta)]^{2M_L+2N}\left(1+\sum_r\langle g_r\rangle+\sum_{r,p}\langle g_r g_p\rangle+\cdots\right). \quad \text{(A7)}$$

The average of the expression in Eq. (A7) over the disorder, which is represented by all the possible ways to choose the spins in each of the random plaquettes, is particularly simple and yields

$$\overline{\mathcal{Z}^2} = 2^{2N}[\cosh(\beta)]^{2M_L}\left[1+\sum_{m=1}^{M_L}\binom{M_L}{m}\langle g_1 \dots g_m\rangle_{\boldsymbol{\sigma},\mathbf{s}}\right] \quad \text{(A8)}$$

so that, since in the limit $N\to\infty$ at fixed m we can write $\binom{M_L}{m} \sim M_L^m = (\alpha_L N)^m$, we have

$$\begin{aligned}2^{2N}[\cosh(\beta)]^{2M_L} \leqslant \lim_{N\to\infty}\overline{\mathcal{Z}^2} \leqslant 2^{2N}[\cosh(\beta)]^{2M_L} \\ \times\left(1+\sum_{m=1}^{\alpha_L N}(\alpha N)^m\langle g_1 \dots g_m\rangle_{\boldsymbol{\sigma},\mathbf{s}}\right). \end{aligned} \quad \text{(A9)}$$

The multiplaquette correlations in Eq. (A9) read in turn

$$\langle g_1 \dots g_m\rangle = \sum_{k=0}^{m}\binom{m}{k}\left\langle\prod_{i=1}^{m-k}[\tau_i+t_i]\prod_{j=m-k+1}^{m}t_j\tau_j\right\rangle_{\boldsymbol{\sigma},\mathbf{s}}. \quad \text{(A10)}$$

In Eq. (A10) the lowest degree correlations are those obtained taking the index $k = 0$; namely they are of the kind $\langle\tau_1 \dots \tau_m\rangle_{\boldsymbol{\sigma}}$ or $\langle\tau_1 \dots \tau_{m-k}\rangle_{\boldsymbol{\sigma}}\langle t_{m-k+1} \dots t_m\rangle_{\mathbf{s}}$. The terms on the right-hand side of Eq. (A10) where a single correlation function appears are vanishing in the thermodynamic limit due to the same argument of Appendix A 1 a. With the same kind of arguments one can show that even the terms $\langle\tau_1 \dots \tau_m\rangle_{\boldsymbol{\sigma}}\langle t_1 \dots t_m\rangle_{\mathbf{s}}$ decay to zero in the thermodynamic limit fast enough to compensate the combinatorial prefactors, yielding finally the desired result

$$\lim_{N\to\infty}(\alpha N)^m\langle g_1 \dots g_m\rangle_{\boldsymbol{\sigma},\mathbf{s}} = 0. \quad \text{(A11)}$$

From Eq. (A9) and Eq. (A11) follows finally

$$\overline{\mathcal{Z}^2} = \overline{\mathcal{Z}}^2 = 2^{2N}[\cosh(\beta)]^{2M_L+2N}. \quad \text{(A12)}$$

2. Additional plaquettes on a regular sublattice: Smallest hyperloop via simulated annealing

In Sec. II B of the paper we mentioned a simulated annealing method to find the smallest hyperloop in the high-temperature expansion of Eq. (4). In order to discuss this

method let us first rewrite the partition function as

$$\begin{aligned}\mathcal{Z} &= \sum_{\{\sigma\}} \exp\left[\beta \sum_p \sigma_{i_p}\sigma_{j_p}\sigma_{k_p}\right] \\ &= [\cosh(\beta)]^N \sum_{\sigma_1,\ldots,\sigma_N} \prod_p \left[1+\tanh(\beta)\sigma_{i_p}\sigma_{j_p}\sigma_{k_p}\right] \\ &= [\cosh(\beta)]^N \sum_{\sigma_1,\ldots,\sigma_N} \prod_p \sum_{n_p=0,1} \left[\tanh(\beta)\sigma_{i_p}\sigma_{j_p}\sigma_{k_p}\right]^{n_p},\end{aligned} \tag{A13}$$

where the index p runs over all the plaquettes of the system, both the plaquettes of the original TPM and the additional plaquettes of the auxiliary sublattice introduced in Sec. II B. In the last line of Eq. (A13) it is convenient to explicitly write the product over the spins:

$$\begin{aligned}\mathcal{Z} &= [\cosh(\beta)]^N \sum_{\sigma_1,\ldots,\sigma_N} \sum_{\{n\}} \left\{ \prod_p [\tanh(\beta)]^{n_p} \right. \\ &\quad \left. \times \prod_i \sigma_i^{(\sum_{p\in\partial i} n_p)_{\mathrm{mod}2}} \right\} \\ &= [\cosh(\beta)]^N \sum_{\{n\}} \left\{ \prod_p [\tanh(\beta)]^{n_p} \right. \\ &\quad \left. \times \prod_i \left[1+(-1)^{(\sum_{p\in\partial i} n_p)_{\mathrm{mod}2}}\right] \right\},\end{aligned} \tag{A14}$$

where now the index p labels the plaquettes around a given spin, $p \in \partial i$. The sum over variables $\{n_i\}_{i=1,\ldots,M}$ appearing in the last lines of Eq. (A14) represents the sum over all possible collections of plaquettes, either forming or not a hyperloop. Within a certain collection of plaquettes the one labeled with p is present when $n_p = 1$ and absent when $n_p = 0$. Let us stress that each collection of plaquettes which does not form a hyperloop, i.e., an assignment of the variables n_p such that, at least for one i, we have $(\sum_{p\in\partial i} n_p)_{\mathrm{mod}2} = 1$, does not contribute to the sum in Eq. (A14). That is why, in order to seek nontrivial terms of $\mathcal{Z}$, we need to find hyperloops. A hyperloop correspond therefore to a choice of $\{n_p\}$ such that for each spin we have

$$\left(\sum_{p\in\partial i} n_p\right)_{\mathrm{mod}2} = 0. \tag{A15}$$

Therefore, in order to find hyperloops, one can look for the ground states of the dual model defined by the following energy function:

$$\mathcal{H}_{\mathrm{dual}}(N) = \sum_{i=1}^{N} \sum_{p\in\partial i} n_p. \tag{A16}$$

The simulated annealing method comes at this stage as the most natural one to seek for the ground states of the Hamiltonian in Eq. (A16). One introduces an effective inverse temperature parameter $\beta_{\mathrm{eff}} = T_{\mathrm{eff}}^{-1}$ and then samples configurations according to the Boltzmann measure $\exp[-\beta_{\mathrm{eff}}\mathcal{H}_{\mathrm{dual}}(N)]$, while slowly decreasing T_{eff}, until a configuration with $E = 0$ is found. In order to find the smallest hyperloop we have realized this simulated annealing search varying the size N of a TPM with an auxiliary sublattice made of side 3 triangles and with open boundary conditions. Varying N we considered always lattices with a side that was a multiple of the incommensurate sublattice cell side; namely we considered triangular lattices of rhomboidal shape and side $L = 6,9,12,\ldots$. The result of our study is that the smallest hyperloop appears in a lattice of side $L = 12$ made of L^2 plaquettes of the TPM and 4^2 plaquettes of the additional sublattice. Such a hyperloop, which is represented in Fig. 3, is made by 54 plaquettes of the TPM model and 10 plaquettes of the additional sublattice.

APPENDIX B: LEAF-REMOVAL EXACT SOLUTION FOR THE RANDOM-DILUTED TPM ON A RANDOM GRAPH

For a random regular graph the action of the "leaf-removal" algorithm is represented in the thermodynamic limit by an infinite set of differential equations [21] for the connectivities of spins, $n_\ell(t)$, where t is the reduced time $t = n/N$, with N the total number of spins in the system and n the number of iterations of the leaf-removal algorithm. Because the maximum possible value taken by n is N the reduced time is in the interval $[0,1]$. Our random-diluted TPM differs from the XOR-SAT because for the latter the initial connectivity $n_\ell(0)$ is Poissonian, while in our case it is the mixed Poissonian/binomial distribution of Eq. (23) in Sec. III of the main text. The probability distribution in Eq. (23) is the only ingredient of the original random-diluted TPM left when the model is studied on the random regular graph. While the behavior of $n_\ell(t;\alpha_s,\alpha_L)$ can be studied analytically on the random graph, for the original RD-TPM model this can be studied only numerically. The differential equations for the evolution of the connectivity under leaf removal are

$$\begin{aligned}\dot{n}_\ell(t) &= -\delta_{\ell 1} + \delta_{\ell 0} + \frac{2}{3(\alpha_s+\alpha_L-t)} \\ &\quad \times [(\ell+1)n_{\ell+1}(t) - \ell n_\ell(t)],\end{aligned} \tag{B1}$$

where $b(t) = [1 - t/(\alpha_s+\alpha_L)]^{1/3}$. The general solution for $\ell \geqslant 2$ is

$$n_\ell(t) = b^{2\ell}(t) \sum_{k=0}^{\infty} n_{\ell+k}(0) \prod_{\rho=0}^{k} (\ell+\rho) \sum_{r=0}^{k} \frac{[-b^2(t)]^r}{r!} \frac{1}{(k-r)!}. \tag{B2}$$

By assuming the distribution in Eq. (23) as initial condition $n_{\ell+k}(0)$ and plugging it into Eq. (B2) one finds for $\ell \geqslant 2$

$$n_\ell(t) = \frac{[3\alpha_L b^2(t)]^\ell}{\ell!} \frac{e^{-3\alpha_L b^2(t)}}{\mathcal{N}} \sum_{r=0}^{3} \mathcal{C}_{r,\ell} B_r(g(t)), \tag{B3}$$

where $B_r(x)$ is the Bell polynomial of order r in the variable $x, g(t) = 3\alpha_L[1 - b^2(t)]$ and the coefficients $\mathcal{C}_{r,\ell}$ are

$$\mathcal{C}_{0,\ell} = \rho_0 + \ell\frac{\rho_1}{3\alpha_L} + \ell(\ell-1)\frac{\rho_2}{(3\alpha_L)^2} + \ell(\ell-1)(\ell-2)\frac{\rho_3}{(3\alpha_L)^3},$$

$$\mathcal{C}_{1,\ell} = \frac{\rho_1}{3\alpha_L} + (2\ell-1)\frac{\rho_2}{(3\alpha_L)^2} + (3\ell^2-6\ell+2)\frac{\rho_3}{(3\alpha_L)^3},$$

$$\mathcal{C}_{2,\ell} = \frac{\rho_2}{(3\alpha_L)^2} + 3(\ell-1)\frac{\rho_3}{(3\alpha_L)^3},$$
$$\mathcal{C}_{3,\ell} = \frac{\rho_3}{(3\alpha_L)^3}. \tag{B4}$$

The probability that a certain spin is a leaf at the iteration t,$n_1(t)$, is then

$$n_1(t) = b^2(t)\left[n_1(0) + \int_0^t ds\left(\frac{4n_2(s)}{3(\alpha_s+\alpha_L-s)} - 1\right)\frac{1}{b^2(s)}\right]. \tag{B5}$$

When the probability to find a leaf vanishes before all the spins are eliminated, i.e., when $n_1(t) = 0$ with $t < 1$, the system has a finite core. On the contrary when $n_1(t) = 0$ only at $t = 0$ there is no core. Studying the behavior of $n_1(t)$ at different values of α_s and α_L it is then possible to locate in the parameter space the line (α_s^{core},α_L^{core}). In order to find the SAT/UNSAT transition one needs then to calculate the number of spins and plaquettes in the core, when it is present. The concentration of spins in the core reads

$$n_c(t) = \sum_{\ell=2}^{\infty} n_\ell(t), \tag{B6}$$

and by plugging the definition of $n_\ell(t)$ from Eq. (B2) into Eq. (B6) one gets

$$n_c(t) = \frac{e^{-g(t)}}{\mathcal{N}}\left[-\mathcal{K}_0(t) + \sum_{r=0}^{3}\mathcal{K}_r(t)[-g(t) + e^{g(t)}B_r(g(t))]\right], \tag{B7}$$

where we have defined $g(t) = 3\alpha_L b^2(t)$ and the coefficients $\mathcal{K}_r(t)$ read as

$$\begin{aligned}
\mathcal{K}_0(t) &= \rho_0 + f(t)\left[\frac{\rho_1}{3\alpha_L} - \frac{\rho_2}{(3\alpha_L)^2} + 2\frac{\rho_3}{(3\alpha_L)^3}\right] \\
&\quad + [f(t) + f^2(t)]\left[\frac{\rho_2}{(3\alpha_L)^2} - 3\frac{\rho_3}{(3\alpha_L)^3}\right] \\
&\quad + [f(t) + 3f^2(t) + f^3(t)]\frac{\rho_3}{(3\alpha_L)^3}, \\
\mathcal{K}_1(t) &= \frac{\rho_1}{3\alpha_L} - \frac{\rho_2}{(3\alpha_L)^2} + 2\frac{\rho_3}{(3\alpha_L)^3} \\
&\quad + 2f(t)\left[\frac{\rho_2}{(3\alpha_L)^2} - 3\frac{\rho_3}{(3\alpha_L)^3}\right] \\
&\quad + [f(t) + f^2(t)]3\frac{\rho_3}{(3\alpha_L)^3}, \\
\mathcal{K}_2(t) &= \left[\frac{\rho_2}{(3\alpha_L)^2} - 3\frac{\rho_3}{(3\alpha_L)^3}\right] + 3\frac{\rho_3}{(3\alpha_L)^3}f(t), \\
\mathcal{K}_3(t) &= \frac{\rho_3}{(3\alpha_L)^3}.
\end{aligned} \tag{B8}$$

The number of plaquettes left in the system at time t in the leaf-removal algorithm is then simply provided by $m_c(t) = \alpha_s + \alpha_L - t$. For each point ($\alpha_s$,$\alpha_L$) in the parameter space one must look for the time t^* at which the leaf-removal algorithm stops and then, if $n_c(t^*) > 0$, consider the ratio $\gamma = m_c(t^*)/n_c(t^*)$; the static transition line is identified by $\gamma = 1$.

APPENDIX C: LEAF REMOVAL AND PARTIAL TRACES

Let us justify here some of the arguments in Sec. III B of the main text. We briefly explain why in the case when leaf removal eliminates all the spins from the interaction network then also the partition function can be summed by means of partial traces without giving rise to any close diagram; this is the case when $\mathcal{Z}$ has the simple expression in Eq. (25) of Sec. III B of the main text. The method of partial traces consists of summing the partition function starting from the open boundaries of the lattice. The necessary condition for this method to work is that each step there is at least one spin belonging to a single plaquette. Let us explain how the iterative summation algorithm works:

(1) Look for a spin which appears in a single plaquette, say σ_0.

(2) Sum over values of the spin σ_0 in the partition function:

$$\begin{aligned}
\mathcal{Z} &= \sum_{\sigma_0,\ldots,\sigma_N} \exp\left(\beta\sum_{\mu=1}^{M_s+M_L}\sigma_{i(\mu)}\sigma_{j(\mu)}\sigma_{k(\mu)}\right) \\
&= \cosh(\beta)\sum_{\sigma_0,\ldots}[1 + \sigma_{0(\nu)}\sigma_{1(\nu)}\sigma_{2(\nu)}\tanh(\beta)] \\
&\quad \times \exp\left(\beta\sum_{\mu\neq\nu}^{M_s+M_L}\sigma_{i(\mu)}\sigma_{j(\mu)}\sigma_{k(\mu)}\right) \\
&= 2\cosh(\beta)\sum_{\sigma_1,\ldots,\sigma_N}\exp\left(\beta\sum_{\mu\neq\nu}^{M_s+M_L}\sigma_{i(\mu)}\sigma_{j(\mu)}\sigma_{k(\mu)}\right).
\end{aligned} \tag{C1}$$

(3) Check whether either $\sigma_{1(\nu)}$ or $\sigma_{2(\nu)}$ in Eq. (C1), or both, are again participating in a single interaction $\gamma \neq \nu$ after the removal of ν by summation. If for instance $\sigma_{1(\nu)}$ is appearing only in $\sigma_{1(\nu)}\sigma_{j(\gamma)}\sigma_{k(\gamma)}$, go back to point 2. If both $\sigma_{1(\nu)}$ and $\sigma_{2(\nu)}$ are participating in more than one interaction, go back to point 1.

(4) If and only if the above recursion can be iterated summing over all the spins of the system the partition function is the one of Eq. (25).

From the description of the method of partial traces, it is clear that it is exactly the iterative scheme of leaf removal. The situation when leaf removal leaves a finite core is the situation where a closed diagram arises in $\mathcal{Z}$, so that $\mathcal{Z}$ cannot be simply summed by means of partial traces. It is worthwhile to recall that in order to use leaf removal or partial traces one must choose the correct boundary conditions; this is due to the deterministic nature of these decimation algorithms. Consider for instance the pure triangular plaquette model with N spins [16]; the partition function is exactly known to be $\mathcal{Z} = 2^N[\cosh(\beta)]^N$. Nevertheless, in the case of periodic boundary conditions there are no leaves (no spins appearing in a single plaquette), so that both the leaf-removal algorithm and the partial-traces iterations cannot be started: it looks like the whole system is a core of dimension N. On the contrary, if one considers open boundary conditions, one finds from partial traces that $\mathcal{Z} = 2^N[\cosh(\beta)]^N$, apart from corrections negligible in the thermodynamic limit. Open boundary conditions are therefore the correct choice if one wants to use this kind of algorithm to study the thermodynamics of the system. Moreover, in a phase diagram like the one of Fig. 6,

open and periodic boundary conditions correspond to the same points, because they differ for a subextensive number of plaquettes.

APPENDIX D: BELIEF-PROPAGATION EQUATIONS FOR THE RANDOM-DILUTED TPM

As mentioned in the main text in Sec. IV, in order to represent the two different kinds of plaquettes in the system, it is convenient to introduce two different cavity fields, $v_{\gamma\to i}$ and $u_{\gamma\to i}$, respectively for the "short" and "long" range plaquettes. These fields allow one to write the marginal probability distribution of the spin i when all interactions around it but γ are removed, with γ representing respectively a short or long range plaquette:

$$p_v(\sigma_i) = \frac{e^{\beta v_{\gamma\to i}\sigma_i}}{2\cosh(\beta v_{\gamma\to i})}, \quad p_u(\sigma_i) = \frac{e^{\beta u_{\gamma\to i}\sigma_i}}{2\cosh(\beta u_{\gamma\to i})}. \tag{D1}$$

In order to write in a clear way the belief propagation (BP) equations, we need to introduce also the couple of cavity fields $\tilde{v}_{i\to\gamma}$ and $\tilde{u}_{i\to\gamma}$, which represent the effective field on σ_i when only the plaquette γ is removed, respectively when γ is short and long range. The belief propagation equations for our model read then

$$\begin{aligned}
\tilde{u}_{j\to\gamma} &= \sum_{\beta\in\partial j\setminus\gamma}^{n_L-1} u_{\beta\to j} + \sum_{\beta\in\partial j\setminus\gamma}^{n_s} v_{\beta\to j},\\
\tilde{v}_{j\to\gamma} &= \sum_{\beta\in\partial j\setminus\gamma}^{n_L} u_{\beta\to j} + \sum_{\beta\in\partial j\setminus\gamma}^{n_s-1} v_{\beta\to j},\\
u_{\gamma\to i} &= \frac{1}{\beta}\tanh^{-1}\left(\tanh(\beta)\prod_{j\in\partial\gamma\setminus i}\tanh(\beta\tilde{u}_{j\to\gamma})\right),\\
v_{\gamma\to i} &= \frac{1}{\beta}\tanh^{-1}\left(\tanh(\beta)\prod_{j\in\partial\gamma\setminus i}\tanh(\beta\tilde{v}_{j\to\gamma})\right),
\end{aligned} \tag{D2}$$

where n_L and n_s denote respectively the number of long and short range plaquettes attached to each spin j. Let us enclose the belief propagation equations in Eq. (D2) in the expression

$$u_{\gamma\to i} = \mathcal{F}(\{u_{\beta\to j}\}_{j\in\partial\gamma\setminus i}). \tag{D3}$$

The population dynamics algorithm is realized starting with a sufficiently large sample of values for each of the two fields u and v, randomly initialized with flat distribution in the interval $[-1,1]$. A random sequential update of the values in the two arrays is realized according to the BP equations in Eq. (D2). The numbers of long, n_L, and short range plaquettes, n_s, attached to each spin and necessary for each iteration step of the algorithm are random variables extracted according to the distributions of Eq. (22) in the text. As is clear from the first two lines of Eq. (D2), at each iteration step one also needs the *excess degree distributions* $p_{\rm exc}$ and $\rho_{\rm exc}$, defined as follows. If we already know that the long-range plaquette γ is attached to the spin σ_i, $p_{\rm exc}$ is the probability that n_L-1 other long-range plaquettes are attached to σ_i. The same is true for the definition of $\rho_{\rm exc}$ when we know that γ is a short-range plaquette. Such distributions read respectively

$$p_{\rm exc}(n_L-1) = \frac{n_L p(n_L)}{\langle n_L\rangle}, \quad \rho_{\rm exc}(n_s-1) = \frac{n_s\rho(n_s)}{\langle n_s\rangle}. \tag{D4}$$

On the Bethe lattice our model has both a dynamic phase transition, at T_d, and a thermodynamic transition, at T_K. While the dynamic ergodicity breaking at T_d disappears in interaction networks with finite loops, the ideal glass transition at T_K may survive. The dynamical transition temperature T_d corresponds to the formation of an exponentially large number of metastable states separated by extensive barriers and such that the system, when initialized in one of this states, is trapped within it. In term of the cavity equations this phenomenon can be recognized by introducing a couple of auxiliary fields $u_{\sigma=\pm1}$ (an $v_{\sigma=\pm1}$) for each type of cavity field (u and v). The cavity fields u_σ represent the value of the field on σ conditioned to the knowledge of the value taken by this spin, either $\sigma=1$ or $\sigma=-1$. If the populations of $u_{\sigma=1}$ and $u_{\sigma=-1}$, which are calculated according to the equations below, Eq. (D5), at equilibrium are such that the $\mathcal{P}(u)=\mathcal{P}_1(u_1)=\mathcal{P}_{-1}(u_{-1})$, where $\mathcal{P},\mathcal{P}_1$, and $\mathcal{P}_{-1}$ are the probability distributions respectively of u,u_{-1} and u_{+1}, it means that the system is in the simple paramagnetic state. On the contrary when the two distributions $\mathcal{P}_1(u_1)$ and $\mathcal{P}_{-1}(u_{-1})$ become different from the distribution $\mathcal{P}(u)$ of the equilibrium field, it means that the system "remembers" the initial condition and the effective field around a certain spin favors the values taken by such spin in the initial condition: ergodicity is dynamically broken. The equation to recursively update the distributions $\mathcal{P}_\sigma(u_\sigma)$ is the following:

$$\begin{aligned}
\mathcal{P}_\sigma(u_\sigma|u) = &\sum_{\{m_L(i),n_s(i)\}}\prod_{i=1}^{2}p_{\rm exc}(m_L(i))\rho(n_s(i))\int\left[\prod_{i=1}^{2}\prod_{j}^{m_L(i)}\prod_{k}^{n_s(i)}du^j dv^k\mathcal{P}(u^j)\mathcal{P}(v^k)\right]\delta(u-\mathcal{F}(\{u^j,v^k\}))\sum_{\sigma_1\sigma_2}\frac{e^{\beta\sigma\sigma_1\sigma_2}}{\mathcal{Z}(\{u^j,v^k\})}\\
&\times\prod_{i=1}^{2}\prod_{j}^{m_L(i)}\prod_{k}^{n_s(i)}\frac{e^{\beta u^j\sigma_i}}{2\cosh(\beta u^j)}\frac{e^{\beta v^k\sigma_i}}{2\cosh(\beta v^k)}\int\left[\prod_{i=1}^{2}\prod_{j}^{m_L(i)}du^j_{\sigma_i}\mathcal{P}_{\sigma_i}(u^j_{\sigma_i}|u^j)\prod_{k}^{n_s(i)}dv^k_{\sigma_i}\mathcal{P}_{\sigma_i}(v^k_{\sigma_i}|v^k)\right]\delta\big(u_\sigma-\mathcal{F}\big(\{u^j_{\sigma_i},v^k_{\sigma_i}\}\big)\big),
\end{aligned} \tag{D5}$$

where $n_s(i)$ is drawn from ρ_n in Eq. (22) while $m_L(i)$ is drawn from $\rho_{\rm exc}$ in Eq. (D4). The same kind of equation holds for $\mathcal{P}_\sigma(v_\sigma|v)$, just with $n_L(i)$ [drawn from p_n in Eq. (22)] in place of $m_L(i)$ and $m_s(i)$ [drawn from $p_{\rm exc}$ in Eq. (D4)] in place of $n_s(i)$.

The iteration step of the population dynamics according to Eq. (D5) proceeds as follows:

(1) Choose an element to update in the population of fields u_σ, which is equivalent to saying: choose randomly a spin σ in the lattice. It is assumed that we are interested in the cavity field on σ that is obtained by removing all the plaquettes but one, say the plaquette γ. When studying the distribution of u_σ we know that γ is a long-range plaquette.

(2) Consider the spins σ_i which are interacting with σ through the plaquette γ. Extract then the number of long-range, $m_L(i)-1$, and short-range, $n_s(i)$, plaquettes attached to each of the spins σ_i.

(3) Compute the cavity field u according to the function $\mathcal{F}$ in Eq. (D3) from the cavity fields $\{u^j, v^k\}$.

(4) Choose the values of spins σ_i according to equilibrium measure for a given value of σ, namely with probability $p(\sigma_1,\sigma_2|\sigma) = \frac{e^{\beta\sigma\sigma_1\sigma_2}}{\mathcal{Z}(\{u^j,v^k\})}\prod_{i=1}^{2}\prod_{j}^{m_L(i)}\prod_{k}^{n_s(i)}\frac{e^{\beta u^j\sigma_i}}{2\cosh(\beta u^j)}\frac{e^{\beta v^k\sigma_i}}{2\cosh(\beta v^k)}$.

(5) For each cavity field u^j (v^k) consider the attached $u^j_{\sigma_i}$ ($v^k_{\sigma_i}$).

(6) From the set of $\{u^j_{\sigma_i}, v^k_{\sigma_i}\}$ update the field u_σ (v_σ) according to $\mathcal{F}$.

Once the population dynamic algorithm is converged and the stationary probability distributions also for the conditioned cavity fields u_σ and v_σ are known, one can calculate from it the free energy within a single metastable state according to the following formula:

$$f_{\rm meta} = \alpha_L\langle f_L(u,v,u_\sigma,v_\sigma)\rangle + \alpha_s\langle f_s(u,v,u_\sigma,v_\sigma)\rangle - \sum_n \mathcal{Q}_n(\alpha_s,\alpha_L)(n-1)\langle f^{(n)}_\sigma(u,v,u_\sigma,v_\sigma)\rangle, \tag{D6}$$

where we have called here $\mathcal{Q}_n(\alpha_s,\alpha_L)$ the mixed Poisson/binomial probability distribution of spin connectivity defined in Eq. (23) as $n_\ell(\alpha_s,\alpha_L)$. The free energy per plaquette reads, in the case of a long-range plaquette, as

$$\begin{aligned}\langle f_L(u,v,u_\sigma,v_\sigma)\rangle = -\frac{1}{\beta}\sum_{\{\sigma_i\},i\in\partial\triangle}\sum_{\{m_L(i),n_s(i)\}}\prod_{i=1}^{3}p_{\rm exc}(m_L(i))\rho(n_s(i))\int\left[\prod_{i=1}^{2}\prod_{j}^{m_L(i)}\prod_{k}^{n_s(i)}du^j dv^k\mathcal{P}(u^j)\mathcal{P}(v^k)\right]\\ \times\frac{e^{\beta\prod_{i=1}^{3}\sigma_i}}{\mathcal{Z}(\{u^j,v^k\})}\prod_{i=1}^{3}\prod_{j=1}^{m_L(i)}\prod_{k=1}^{n_s(i)}\frac{e^{\beta u^j\sigma_i}}{2\cosh(\beta u^j)}\frac{e^{\beta v^k\sigma_i}}{2\cosh(\beta v^k)}\\ \times\int\left[\prod_{i=1}^{2}\prod_{j}^{m_L(i)}du^j_{\sigma_i}\mathcal{P}_{\sigma_i}\left(u^j_{\sigma_i}|u^j\right)\prod_{k}^{n_s(i)}dv^k_{\sigma_i}\mathcal{P}_{\sigma_i}\left(v^k_{\sigma_i}|v^k\right)\right]\ln\mathcal{Z}_\triangle\left(\left\{u^j_{\sigma_i},v^k_{\sigma_i}\right\}\right).\end{aligned} \tag{D7}$$

The expression in Eq. (D7) has to be consistently modified for a short-range plaquette. The free energy per spin is then

$$\begin{aligned}\langle f^{(n)}_\sigma(u,u_1,u_{-1})\rangle = \sum_{\{\sigma\}}\int\left[\prod_{j}^{m_L}\prod_{k}^{n_s}du^j dv^k\mathcal{P}(u^j)\mathcal{P}(v^k)\right]\frac{1}{\mathcal{Z}(\{u^j,v^k\})}\prod_{j=1}^{m_L}\prod_{k=1}^{n_s}\frac{e^{\beta u^i\sigma}}{2\cosh(\beta u^i)}\frac{e^{\beta v^k\sigma}}{2\cosh(\beta v^k)}\\ \times\int\left[\prod_{j}^{m_L(i)}du^j_{\sigma_i}\mathcal{P}_{\sigma_i}\left(u^j_{\sigma_i}|u^j\right)\prod_{k}^{n_s(i)}dv^k_{\sigma_i}\mathcal{P}_{\sigma_i}\left(v^k_{\sigma_i}|v^k\right)\right]\ln\mathcal{Z}_\sigma\left(\left\{u^j_\sigma,v^k_\sigma\right\}\right).\end{aligned} \tag{D8}$$

The two partition functions $\mathcal{Z}_\triangle$ and $\mathcal{Z}_\sigma$ appearing respectively in Eq. (D7) and Eq. (D8) are defined as

$$\begin{aligned}\mathcal{Z}_\triangle\left(\left\{u^j_{\sigma_i},v^k_{\sigma_i}\right\}\right) &= \sum_{\{\sigma_i\}}e^{\beta\prod_{i=1}^{3}\sigma_i}\prod_{i=1}^{3}\prod_{j=1}^{m_L(i)}\prod_{k=1}^{n_s(i)}\frac{e^{\beta u^j\sigma_i}}{2\cosh(\beta u^j)}\frac{e^{\beta v^k\sigma_i}}{2\cosh(\beta v^k)},\\ \mathcal{Z}_\sigma\left(\left\{u^j_{\sigma_i},v^k_{\sigma_i}\right\}\right) &= \sum_{\sigma}\prod_{j=1}^{m_L}\prod_{k=1}^{n_s}\frac{e^{\beta u^j\sigma}}{2\cosh(\beta u^j)}\frac{e^{\beta v^k\sigma}}{2\cosh(\beta v^k)}.\end{aligned} \tag{D9}$$

The free energy in the paramagnetic phase is the same as in the high-temperature expansion,

$$f_{\rm para} = -\beta^{-1}\ln(2) - \beta^{-1}(\alpha_s+\alpha_L)\ln\cosh(\beta). \tag{D10}$$

The configurational entropy can be finally obtained as

$$\Sigma = \beta(f_{\rm meta} - f_{\rm para}). \tag{D11}$$

[1] T. R. Kirkpatrick, D. Thirumalai, and P. G. Wolynes, Phys. Rev. A **40**, 1045 (1989).

[2] M. Mézard and G. Parisi, J. Phys.: Condens. Matter **12**, 6655 (2000).

[3] V. Lubchenko and P. G. Wolynes, Annu. Rev. Chem. **58**, 235 (2007).

[4] G. Parisi and F. Zamponi, Rev. Mod. Phys. **82**, 789 (2010).

[5] Juan P. Garrahan, P. Sollich, and C. Toninelli, *Dynamical Heterogeneities in Glasses, Colloids, and Granular Media* (Oxford University Press, Oxford, 2011).
[6] G. H. Fredrickson and H. C. Andersen, Phys. Rev. Lett. **53**, 1244 (1984).
[7] S. Eisinger and J. Jäckle, Z. Phys. B **84**, 115124 (1991).
[8] W. Kob and H. C. Andersen, Phys. Rev. E **48**, 4364 (1993).
[9] A. Lipowski and D. Johnston, J. Phys. A **33**, 4451 (2000).
[10] H. Yin and B. Chakraborty, Phys. Rev. E **65**, 036119 (2002).
[11] M. Sellitto, J. Chem. Phys. **138**, 224507 (2013).
[12] S. Franz and M. Sellitto, J. Stat. Mech. (2013) P02025.
[13] M. Sellitto, G. Biroli, and C. Toninelli, Europhys. Lett. **69**, 496 (2005).
[14] L. Foini, F. Krzakala, and F. Zamponi, J. Stat. Mech. (2012) P06013.
[15] M. E. J. Newman and C. Moore, Phys. Rev. E **60**, 5068 (1999).
[16] J. P. Garrahan and M. E. J. Newman, Phys. Rev. E **62**, 7670 (2000).
[17] R. L. Jack, L. Berthier, and J. P. Garrahan, Phys. Rev. E **72**, 016103 (2005).
[18] R. L. Jack and J. P. Garrahan, J. Chem. Phys. **123**, 164508 (2005).
[19] J. P. Garrahan, Phys. Rev. E **89**, 030301(R) (2014).
[20] R. M. Turner, R. L. Jack, and J. P. Garrahan, Phys. Rev. E **92**, 022115 (2015).
[21] M. Mezard, F. Ricci-Tersenghi, and R. Zecchina, J. Stat. Phys. **111**, 505 (2003).
[22] A. Barrat and M. Weigt, Eur. Phys. J. B **13**, 547 (2000).
[23] S. Franz, M. Mezard, F. Ricci-Tersenghi, M. Weigt, and R. Zecchina, Europhys. Lett. **55**, 465 (2001).
[24] A. Cavagna, Phys. Rep. **476**, 51 (2009).
[25] F. Ricci-Tersenghi, M. Weigt, and R. Zecchina, Phys. Rev. E **63**, 026702 (2001).
[26] B. Derrida, Phys. Rev. B **24**, 2613 (1981).
[27] A. B. Bortz, M. H. Kalos, and J. L. Lebowitz, J. Comput. Phys. **17**, 10 (1975).
[28] D. Alvarez, S. Franz, and F. Ritort, Phys. Rev. B **54**, 9756 (1996).
[29] A. Cavagna, I. Giardina, and T. Grigera, Europhys. Lett. **61**, 74 (2003).
[30] A. Cavagna, I. Giardina, and T. S. Grigera, J. Chem. Phys. **118**, 6974 (2003).
[31] B. Wemmenhove, T. Nikoletopoulos, and J. P. L. Hatchett, J. Stat. Mech. (2005) P11007.
[32] C. Toninelli, G. Biroli, and D. S. Fisher, Phys. Rev. Lett. **96**, 035702 (2006).
[33] C. Toninelli and G. Biroli, J. Stat. Phys. **130**, 83 (2008).
[34] G. Biroli and C. Toninelli, Eur. Phys. J. B **64**, 567 (2008).
[35] M. Jeng and J. M. Schwarz, Phys. Rev. E **81**, 011134 (2010).
[36] A. Ghosh, E. Teomy, and Y. Shokef, Europhys. Lett. **106**, 16003 (2014).